3 Scintillation Mechanisms in Inorganic Scintillators

Abstract. Details of energy transfer phenomena and scintillation mechanisms in luminescent media excited by ionizing radiation are discussed in this chapter. The sequence of relaxation of electronic excitations is described: creation of electron-hole pairs, energy transfer to emitting centers of interest and quantum efficiency of these luminescent centers. The theoretical limit of the light yield is usually much higher than the experimental one. The limiting factors at each step of relaxation are considered in self-activated, doped and cross-luminescent scintillation materials. The final stage of luminescent center excitation mechanism in scintillators has a strong influence on the scintillation parameters. It is discussed in detail here. Finally, different examples are given of charge transfer and non-radiative relaxation processes of the scintillating centers through their coupling with the crystal lattice.

3.1 Introduction: How to Answer High Light Yield, Short Decay Time, and Good Energy Resolution

The demand for new and better scintillating materials is very strong for many kinds of applications. Of course, there is no unique best scintillator. Depending on the particular requirements of the application considered, different scintillators would be preferred.

Among the desirable properties of a good scintillator, high efficiency, fast scintillation, and good energy resolution are of most importance in a number of cases.

As it will be demonstrated in the next paragraphs, the light yield depends on many parameters that play a role in the three stages of relaxation of electronic excitations: creation of electron–hole pairs, energy transfer to emitting centers of interest, and quantum efficiency of these centers. The theoretical limit of the light yield is usually much higher than the experimental one. The optimization of scintillators in terms of light efficiency will consist to play with these parameters, which strongly influence the scintillation process.

The scintillation kinetics depends essentially on the energy transfer and the nature of the luminescence centers. In doped materials, the choice for the dopant ion determines the range of time response of the scintillator. For nanosecond time scale response, only few ions are of interest, those exhibiting parity-allowed emission transitions like $5d$–$4f$ transitions of rare-earth ions. Intrinsic fluorescence centers can also exhibit fast fluorescence.

The energy resolution R is the ability for a scintillator to distinguish radiations of slightly different energies. It is usually described as a function of different contributions:

$$R^2 = R_{\mathrm{np}}^2 + R_{\mathrm{inh}}^2 + R_{\mathrm{tr}}^2 + R_{\mathrm{lim}}^2$$

R_{np} is a factor of nonproportionality, which accounts to the fact that in some scintillators, the number of emitted photons is not proportional to the incident energy. Then, secondary electronic excitations of various energies lead to a distribution of light yields, which increases the energy resolution. R_{inh} is related to the inhomogeneity of the crystal, inducing local variations of the light efficiency. R_{tr} is related to the efficiency of the light collection by the detector (usually a photomultiplier PM). R_{lim} is the intrinsic resolution of the detector, described by the well-known Poisson law.

$$R_{\mathrm{lim}} = 2.35\sqrt{\frac{1 + v\,(\mathrm{PM})}{N_{\mathrm{phe}}}}\ ,$$

where $v(PM)$ is the variance of the photomultiplier gain and N_{phe} is the number of photoelectrons emitted by the *PM*.

For an ideal scintillator, the first three contributions are negligible and R_{lim} gives the energy resolution. The light yield being proportional to N_{phe}, a good energy resolution, requires a high light yield.

In many cases, the energy resolution R is actually larger than the theoretical limit R_{lim}. The inhomogeneity of the crystal can be reduced and often cancelled by improving the crystal growth conditions and the light collection can be improved as well. On the other hand, the nonproportionality is a puzzling problem, much more difficult to solve because its origin is not well understood yet. For example, while known scintillators such as cerium-doped orthoaluminates or lanthanum halides compounds exhibit a weak nonproportionality, cerium-doped silicates are strongly "nonproportional." It seems that the structure more than the composition of the crystal may influence the nonproportional behavior.

3.2 Relaxation of Electronic Excitations

Relaxation of electronic excitations involves complex mechanisms. A description of multiplication and thermalization processes has been proposed by different authors using various models (see recent reviews [1–3] and references therein). The purpose here is not to go into the details of phenomenological models, nor to discuss their merit but rather to use simple schemes of relaxation of electronic excitations deduced from simulations and which account qualitatively for the energy distribution and space correlation of excitations. These schemes, first proposed by Vasil'ev, use the band structure of the material. They provide a pedagogical description of the various steps of relaxation

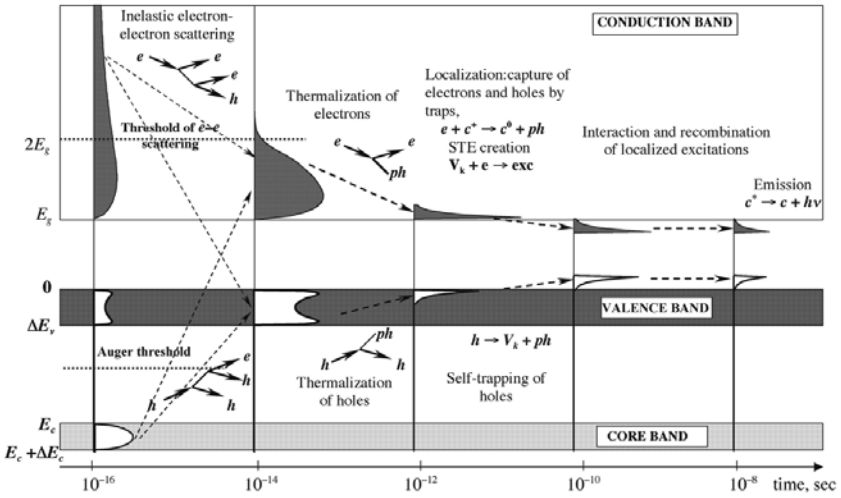

Fig. 3.1. General scheme of relaxation of electronic excitations in an insulator with two channels of relaxation. e for electrons, h for holes, ph for phonons, hν for photons, V_k for self-trapped holes, c_i^n for ionic centers with charge n

from the primary high-energy excitation to final process of light emission by luminescent centers.

A general scheme is represented in Fig. 3.1. For simplicity, only one core band is represented with top energy E_c and bandwidth ΔE_c. The valence band (top energy $E_\mathrm{v} = 0$ and bandwidth ΔE_v) and the conduction band (bottom energy E_g) are separated by the forbidden band of the insulator (band gap width E_g). Five main stages can be considered.

The first one starts with the production of primary excitations by interaction of ionizing particles with the material. For very high incident particle energy, the excitations are essentially deep holes h created in inner-core bands and hot electrons e in the conduction band. Then, in a very short time scale ($10^{-16} - 10^{-14}$s), a large number of secondary electronic excitations are produced through inelastic electron–electron scattering and Auger processes with creation of electrons in the conduction band and holes in core and valence bands. At the end of this stage, the multiplication of excitations is stopped. All electrons in the conduction band have an energy smaller than $2E_\mathrm{g}$ (e–e scattering threshold) and all holes occupy the valence band if there is no core band lying above the Auger process threshold (general case).

The second stage is thermalization of electronic excitations with production of phonons, leading to low kinetic energy electrons in the bottom of the conduction band and of holes in the top of the valence band.

The next stage is characterized by the localization of the excitations through their interaction with stable defects and impurities of the material. For example, electrons and holes can be captured by different traps or

self-trapped in the crystal lattice. Excitons, self-trapped excitons, and self-trapped holes (V_K centers) can be formed with emission of phonons. Localization of excitations can be sometimes accompanied by displacements of atoms (defect creation, photostimulated desorption).

The two last steps are related with migration of relaxed excitations and radiative and/or nonradiative recombination. It is important to consider the interaction between excitations themselves, which can result in the decrease of the number of excitations. This point, which will be discussed later in the next paragraph, is responsible for density effects, nonproportionality of energy response of scintillator, and nonexponential decay kinetics. The very last stage describes the luminescence of emitting centers excited by the final electronic excitations (correlated electron–hole pairs, excitons, separated electrons, holes, etc.) through sequential capture of charge carriers or various energy transfers.

The general scheme of Fig. 3.1 describes the scintillation mechanisms in the case of ionic crystals with simple energy structure. However, important groups of scintillators exhibit a more complicated band structure.

It is, in particular, the case of crystals containing rare earth. For example, in cerium-based or cerium-doped compounds, cerium $4f$ and $5d$ levels fall within the forbidden energy band gap. They must be involved in the scheme of relaxation of electronic excitations because they may play an important role in the scintillation processes (Fig. 3.2). Indeed, rare-earth ions (RE) can be directly excited through impact excitation provided that their concentration is large (it is particularly true for fully concentrated rare-earth compounds). But this excitation is efficient only by electrons with kinetic energies above

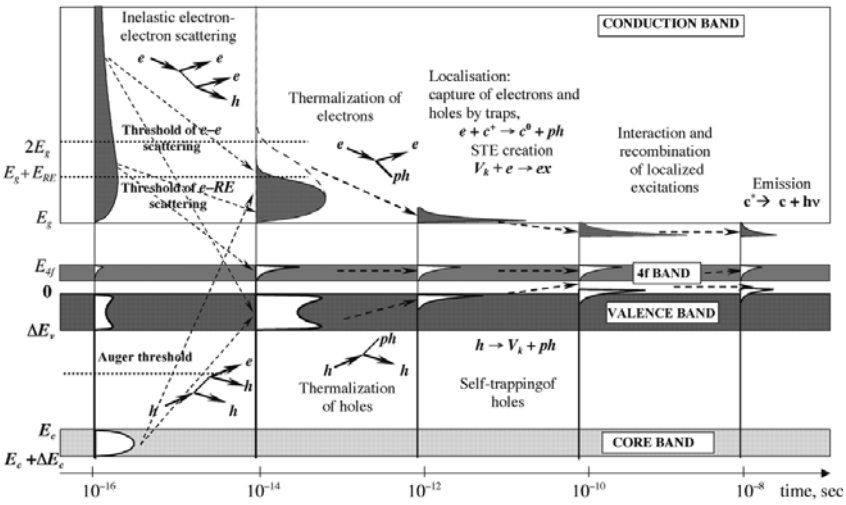

Fig. 3.2. Scheme of relaxation of electronic excitations in rare earth containing crystals

the threshold of e–RE scattering and below the threshold of e–e scattering. In this case, the production of electron–hole pairs with holes in the valence band is not possible. When this process occurs, it is strongly dominant since the density of states in the valence band is much higher than that in rare-earth bands.

This additional pathway of excitation for rare-earth luminescent ions is not detrimental to the creation of electron–hole pairs since it involves electrons with kinetic energy lower than the threshold of e–e scattering and which cannot produce more electronic excitations. Therefore, it would be expected a high light yield for rare-earth crystal scintillators.

Actually, it is not so simple because other factors must be taken into account which can limit the scintillation efficiency and which will be analyzed later.

Cross-luminescent materials belong to another class of scintillators. The mechanisms will be described in more details in the next paragraph. In the scheme of the relaxation of electronic excitations of cross-luminescent systems for which core-valence transition is responsible for a fast subnanosecond luminescence (archetype: BaF_2 with 5pBa as outermost core band), the outermost core band, lying less than $2E_g$ below the bottom of the conduction band, must be taken into account in the representation of the electronic structure (Fig. 3.3). In the first stage is represented the threshold of e–e scattering with production of outermost core band holes ch, at higher energy than that of e–e scattering with production of valence band holes h and anion excitons. At the end of this stage coexist two types of holes since ch cannot relax into the valence band through Auger effect, which is energetically forbidden. After thermalization, localization and eventually interaction of excitations, ch

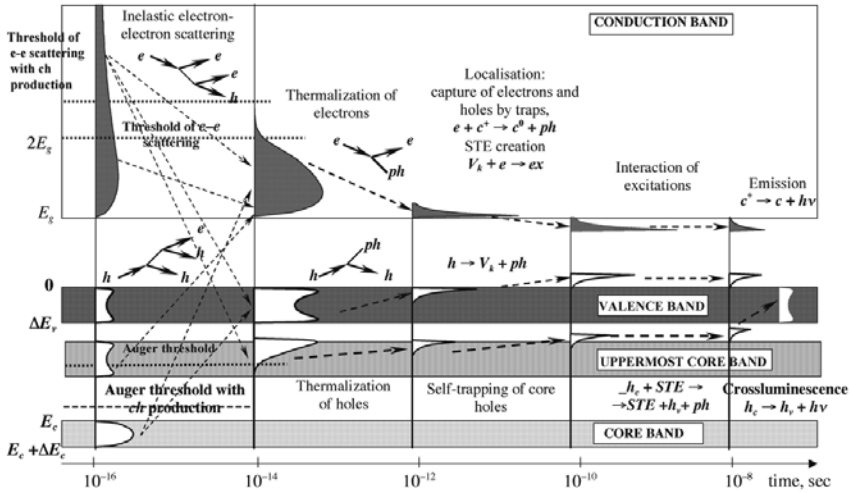

Fig. 3.3. Scheme of relaxation of electronic excitations in cross-luminescent crystals

and h, and self-trapped anion exciton STE can coexist during a relatively long period. In the last stage, only core band holes ch are responsible for cross-luminescence.

3.3 Limiting Factors at Each Step of the Energy Relaxation

The formula for light yield Y mentioned in Chap. 2 also may be expressed as the product of three factors [1, 4]:

$$Y = N_{\mathrm{eh}} SQ \tag{3.1}$$

N_{eh} is the conversion efficiency expressed as a number of electron–hole pairs or excitons, S is the probability of transfer to emitting centers, and Q is the luminescence quantum yield.

These three processes can be considered as successive events, which can be related to the different stages of relaxation of electronic excitations previously described in Sect. 3.2. Let us consider the factors, which limit the scintillator light, yield at each of these three processes.

3.3.1 Creation of Electronic Excitations

Electronic excitations, which are potentially available in the scintillator as donors in the transfer process to luminescence centers, are produced during the first two stages described in Figs. 3.1–3.3: multiplication and thermalization stages.

$\mathrm{N_{eh}}$ is usually expressed via the average energy $\mathrm{E_{eh}}$ required for the creation of a thermalized e–h pair. Considering $\mathrm{E_{inc}}$ as the energy deposited by an ionizing particle, we have

$$N_{\mathrm{eh}} = \frac{E_{\mathrm{inc}}}{E_{\mathrm{eh}}} \tag{3.2}$$

The first estimations of E_{eh} around (2–3)E_{g}, E_{g} being the forbidden energy band gap, were made quite some time ago [5,6]. It is therefore obvious that the parameter, which limits the production of electron–hole pairs and excitons, is E_{g}; the larger it is, the lower is N_{eh}.

It should be noted that N_{eh} is a relevant factor only in the case of a simple insulator such as that described in Fig. 3.1. But in crystals with more complicated electronic structure, additional types of excitations can be created, or/and all the electron–hole pairs and excitons are not useful excitations leading to scintillation. For these systems, the light yield η predicted by formula (3.1) deduced from empirical models is usually much larger than the experimentally observed scintillation yield.

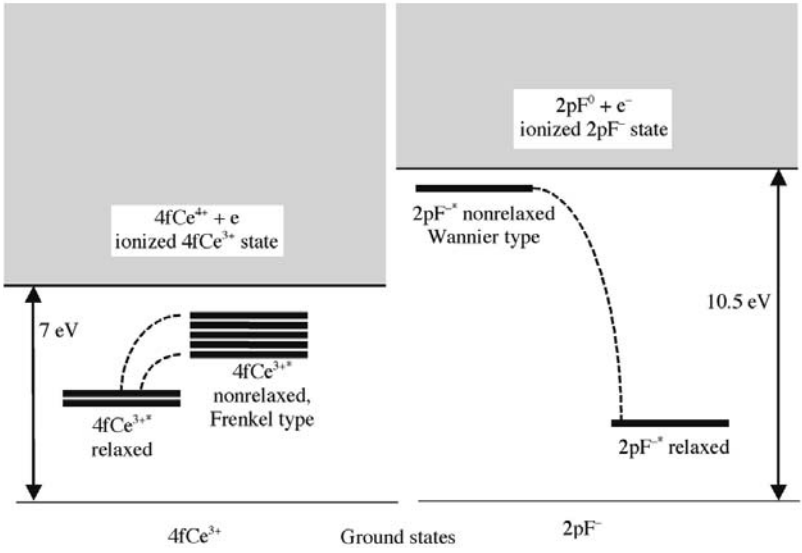

Fig. 3.4. Simplified scheme of coexistence of two types of excitons in cerium fluoride

3.3.1.1 Case of Cerium Compounds

CeF_3 is a model system for analyzing the scintillation mechanisms in ionic crystals and many studies have been devoted to this scintillator (see, for example, [3, 7–22]).

In cerium compounds, cerium $4f$ levels fall within the forbidden band-gap. As a result, two types of excitons can be formed: Ce Frenkel excitons and anion Wannier exciton. A simplified scheme (Fig. 3.4) shows that rare-earth ion excitation is not efficient through energy transfer from anion exciton as well as through sequential capture of holes and electrons by Ce^{3+} ions as demonstrated later in Subsect. 3.3.2.1.

"Useful" excitations can be produced only through impact excitation and only by electrons with kinetic energies in a narrow band between the two thresholds of e–e scattering and of e-RE scattering (Fig. 3.2). For such system, it is clear that the number of scintillation-active excitations cannot be estimated by expression (3.1). In fact, the number of useful excitations is reduced by a factor of around 5 in CeF_3. This fact partially explains the relatively low yield of CeF_3.

3.3.1.2 Case of Scintillators with Core-Valence Transitions

Systems with high-lying outermost core bands can give rise to so-called cross-luminescence involving core-valence transitions [23]. For example, in the case of BaF_2, a Ba^{2+} 5p core hole can decay only radiatively and not via an Auger process. Cross-luminescence is very sensitive to track effects [24–27].

Therefore, the scintillation efficiency can be calculated using expression (3.1) only if the conversion efficiency is expressed as the number of Ba^{2+} 2p core holes rather than as the total number of excitations [22].

3.3.2 Transfer to Luminescence Centers

This process involves the third and fourth stages of relaxation of electronic excitations described previously in Figs. 3.1–3.3. It is a very critical part of the scintillation mechanism since electron–hole pairs or excitons can be affected by many events during their migration and before they interact with luminescence centers, and can result in nonradiative recombination. This can limit the number of effective donors in the energy transfer processes to the acceptors and substantially change as well as the time dependence of the scintillation.

3.3.2.1 Limitation in Charge Carriers Capture Probability

When donors are electron–hole pairs, the usual channel of excitation for acceptors is a charge transfer process with a sequential capture of charge carriers. For scintillators with high light yield, the capture efficiency must be high. It is, for example, the case of Na- and Tl-doped CsI crystals for which the scintillation emission originates from perturbed or impurity-trapped exciton centers, which are efficiently excited because of the enhanced cross section for electron, capture at Tl^+ and Na^+ impurities [28, 29]. In Ce^{3+}-doped or based-crystals, the hole is first captured and its capture probability strongly depends on the position of the Ce $4f$ level in the forbidden band gap. In cerium-doped oxides and halides, Ce $4f$ level is usually lying very low in the gap close to the top of the valence band [16], and these systems can lead to very efficient scintillation (LSO, LuAP, $LaCl_3$, etc.). On the other hand, Ce^{3+}-doped fluoride crystals cannot exhibit very high light yield because Ce 4f is lying around 3–4 eV above the valence band [16] and the hole capture probability is low. It should be noted that in CeF_3, the Auger cascade over Ce core levels is terminated by the transfer of the hole to the fluoride valence band because the probability of the forbidden Auger transition Ce 4p–Ce $4f$ is very low [3]. It was shown before that the main channel of Ce excitation is through impact by electrons. Excitons can transfer their energy to luminescence centers as well. The dominant process is then nonradiative energy transfer.

3.3.2.2 Specific Killer Ions

The presence of specific ions with active luminescent centers is sometimes undesirable and incompatible with the emission of intense scintillation. These ions can exist as impurities or be constituent of the material. In the case of

impurities, their nature and concentration depend on the purity of starting materials and/or the techniques used for the crystal elaboration. They can compete with active ions for the capture of charge carriers and/or interact with them, and induce severe limitations in scintillation efficiency.

For example, in cerium-doped or cerium-based crystals, in general, the presence of ions with two or more stable valences is harmful. It is due to the fact that cerium itself has two stable valence states Ce^{3+} and Ce^{4+} and can exchange electrons through a metal–metal charge resulting to mutual quenching transfer process. Ce-doped tungstates and vanadates do not exhibit cerium scintillation because of Ce-W and Ce-V interaction of this type [30].

It is known that simultaneous presence of Yb and Ce leads to their mutual fluorescence quenching [31, 32]. Ce^{3+} is a good hole trap and Yb^{3+} a good electron trap. It is a consequence of a particular stability of empty Ce^{4+} $4f$ shell and of totally filled Yb^{2+} 4f shell. In the presence of electron–hole pairs, the initial state (Ce^{3+} Yb^{3+}), after capture of holes by Ce^{3+} and electrons by Yb^{3+} pass by an intermediate (Ce^{4+} Yb^{2+}) excited state and after relaxation and tunnel electron exchange, returns nonradiatively to the initial state.

Quenching of the same type can occur for other couples such as Ce^{3+} + Eu^{3+}, Ce^{3+} + nitrate, and Ce^{3+} + carboxylate ([33] and references therein).

Recently, a new very promising scintillator was discovered: cerium-doped lutetium pyrosilicate crystal (LPS) $Lu_2Si_2O_7$:Ce [34]. This material exhibits a very high light yield when it is grown by the melting zone technique, while its scintillation is absent or very weak when it is elaborated by the Czochralski method. From EPR measurement, it was shown that the quenching of Ce fluorescence is due to the presence of Ir^{4+} impurity ions introduced by the crucible [35]. The mechanisms of quenching have not been elucidated yet, but it could be related to a charge transfer process between Ce^{3+} and Ir^{4+} ions.

In cerium-doped systems, Ce^{3+} and Ce^{4+} centers can coexist. Ce^{4+} has no electron in the $4f$ shell, but can be excited through a charge transfer process after capture of an electron from the valence band. The charge transfer state ($Ce^{3+} + h_v$) relaxes nonradiatively to the ground state. The presence of Ce^{4+} nonradiative recombination centers must be avoided in Ce-doped scintillators. In the case of fluorides, crystal growth under vacuum in reducing atmosphere is a solution to eliminate Ce^{4+} ions. In oxides, when it is possible, annealing in reducing atmosphere can be used. Co-doping with 4+ ions can give good results as well.

3.3.2.3 Self-Trapping, Trapping, Creation of Defects

Self-trapping is a very frequent process in insulating materials. For example, self-trapping holes, so-called V_K centers, can be formed, leading to a decorrelation of electrons and holes. Recombination of electrons with mobile V_K centers [$V_K + e^-$] close to luminescent centers can excite them. Self-trapped excitons (STE) can be formed as well directly from electron–hole

pairs or by trapping electrons in the V_K centers. STE can exhibit luminescence and transfer its energy to luminescent centers. Self-trapping is an intrinsic property of materials. It can strongly influence the efficiency and the time dependence of the scintillation. To interpret the scintillation properties of cerium-doped $LaCl_3$, $LuBr_3$, and $LuCl_3$, O. Guillot-Noël et al. [36] proposed a model involving three different mechanisms which correspond to three different energy transfer processes and which appear at different time ranges: very fast energy transfer by direct correlated electron–hole capture on Ce^{3+}, fast energy transfer by binary electron–hole recombination ($[V_K + e^-]$ on Ce^{3+}) and slower energy transfer by diffusion of STE. They were able to evaluate the relative contribution of the mechanisms through the analysis of the scintillation decay profiles and of the X-ray–induced emission spectra. Their model works well in the case of Ce-doped LaF_3. For the other systems, the temperature dependence of the total yield cannot be explained at low temperature where it is observed a strong quenching. This quenching is probably due to trapping effect, which was not taken into account in their model.

Indeed, some of the electrons and holes can be trapped at more or less deep trapping levels and cannot excite directly luminescent centers through sequential capture but eventually indirectly after releasing from the traps. As a result, a strong luminescent quenching and very long components in the fluorescence decays can be observed in the temperature region of glow peaks. It has been demonstrated that this quenching phenomenon occurs for the X-ray–excited charge transfer luminescence of ytterbium containing aluminum garnets [37, 38].

3.3.2.4 Interaction of Excitations

It was shown through the study of a number of crystals excited by photons of high energy (VUV and X-excitations) using synchrotron radiation that the relaxation of primary electron and hole in a crystal leads in general to the formation of nanometric scale regions containing several electronic excitations separated by short distances. The interaction between closely spaced electronic excitations may lead to luminescence quenching so-called local density–induced quenching [12, 24, 39, 40].

Examples of interactions between closely spaced electronic excitations in an insulator are illustrated in Fig. 3.5. They all produce emission of phonons. An exciton may disappear after interaction with a close low-energy electron e or hole h (processes 1 and 2), a core hole c may interact with a low-energy electron through dipole–dipole or Fano process and low-energy electron and hole are formed (mechanisms 3 and 4), interaction of a core hole with a valence band hole may lead to two valence band holes (mechanism 5). If two excitons interact, one may disappear and the other one may gain energy and reach a higher excited state or disintegrate into an electron–hole pair. Finally, the electron–hole pair can be bound into an exciton again or the components

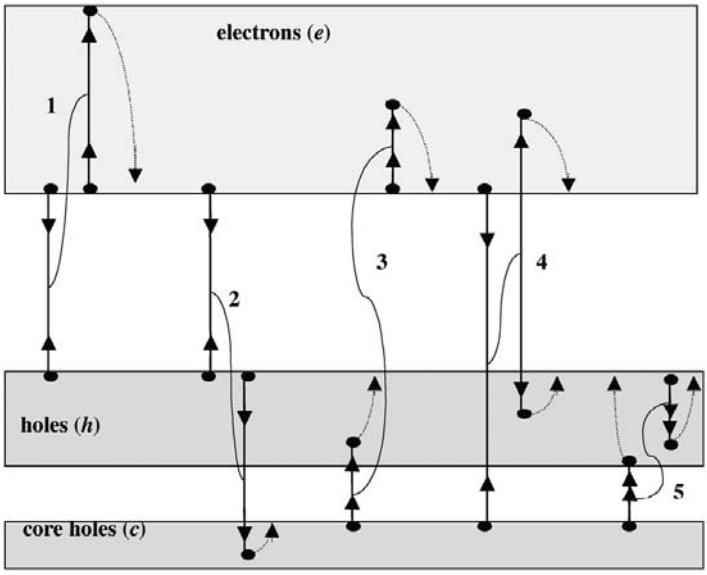

Fig. 3.5. Possible interactions between closely spaced electronic excitations in an insulator. Arrows pointing toward each other show recombination processes, in opposite direction: creation of electronic excitations, in the same direction: increase in the electronic excitation energy. Thin curves denote the interaction, and dotted arrows: electronic excitation thermalization

can decay independently. It should be noted that interaction can be not only of dipole–dipole type, but of other types such as exchange, tunneling, Fano, etc., which strongly depend on the excitations distance and are controlled by the overlap of wave functions of the interacting particles. For dipole–dipole interaction, the interaction radius is 1 to 5 nm; for other types of interaction, it is less than 1 nm.

For electronic excitations created in different events of photon absorption, the probability to be created at such short distances is very low for nonlaser densities of excitation. On the contrary, secondary electronic excitations created by inelastic scattering of photoelectrons or Auger decay of core holes can be quite closely spaced. The process is illustrated in Fig. 3.6. The hot electron relaxes through inelastic electron–electron scattering with creation of secondary excitations. The spatial distribution of such excitations is governed by the diffusion length, which depends on the hot electron energy according to a nonmonotonous function. It is therefore possible to obtain a nonuniform spatial distribution of electronic excitations. The core holes relax according to the Auger mechanism, but in this case, the excited regions are much smaller because the mobility of holes is much smaller in insulating materials. Figure 3.6 shows regions of different sizes (typically 1–5 nm) containing several (4–7) electronic excitations. In these clusters of high local

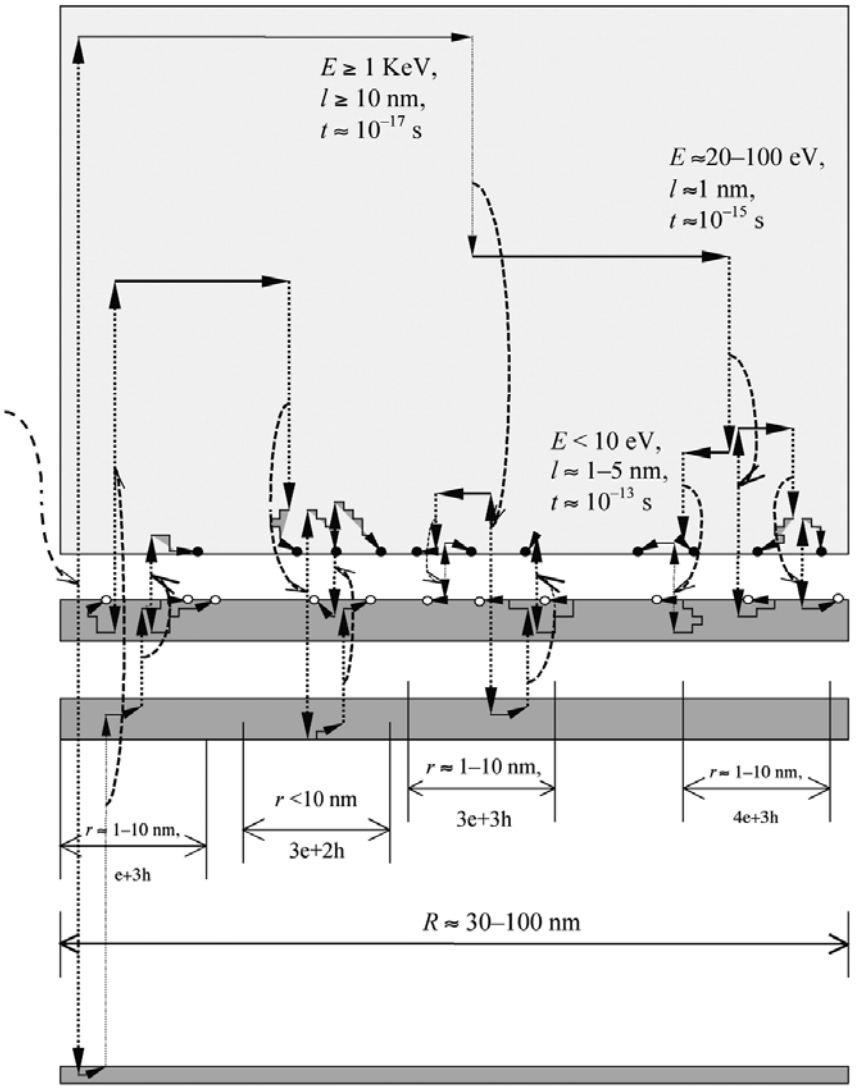

Fig. 3.6. Spatial distribution of electronic excitations created by the absorption of a high-energy photon. The notations are similar to the ones used in Fig. 3.5. Solid circles are electrons; open circles are holes after thermalization. Energy, temporal, and spatial scale characteristics for the process are presented, as well as the composition and dimension of clusters of excitations

e and h density, the interaction between excitations can modify their localization and can even create defects in crystals. In addition, these clusters can excite close luminescent centers, and their interaction is responsible for the acceleration of the fluorescence kinetics and total or partial luminescence quenching. The first evidence of such effect was observed in CeF_3 [41].

Peculiar fast intrinsic luminescence observed in alkali halides, and in particular in CsI, was shown to be the result of interaction of several electron–hole pairs at the initial stage of relaxation [42, 43]. The probability of the effects of correlated relaxation of electronic excitations with the creation of an emission center depends on the crystal and can be quite high. It is clear that the estimation of the light output of scintillators such as CeF_3 or CsI must take into account the role played by regions of high densities of excitation. For example, in the case of CeF_3, interaction of excitations is estimated to reduce the light output by a factor of 2 to 5.

3.3.3 Emission of Luminescent Centers

This process occurs after excitation of the emitting centers. It is the very last stage of relaxation of electronic excitations. The emission mechanisms depend on the electronic structure of both luminescent ions and crystal lattice in which they are imbedded, and on their mutual interaction.

At this stage, there are many processes, which may limit the luminescence efficiency. Some are related with nonradiative transitions, others with energy transfer. Most of them are well known and it is of interest here to list the main ones, which will be analyzed in more detail in next paragraphs.

3.3.3.1 Electron–Phonon Coupling

Ions in a host lattice interact with the vibrations of the lattice, inducing nonradiative transitions. Whatever the strength of the coupling, there is always a competition between radiative and nonradiative transitions. The quantum efficiency, defined as the ratio of the number of emitted quanta to the number of absorbed quanta, is 1 in the absence of competing radiation less transitions. It is usually the case for luminescent ions in efficient scintillators. In case of intermediate and strong coupling strength, the Stokes shift can induce thermal quenching. In case of weak coupling strength, for which the Stokes shift is absent, nonradiative process can occur through multiphonon emission. In any case, the presence of intermediate excited states between the emitting level and the ground state is harmful because it is a source of nonradiative relaxation. As a matter of fact, Tl^+, Bi^{3+}, or Ce^{3+} ions, which exhibit large free gap below their $6p$ or $5d$ emitting levels, are much more efficient luminescence centers than, for example, $5d \rightarrow 4f$ luminescence Pr^{3+} ions where many $4f$ levels are lying between $5d$ and the ground state.

3.3.3.2 Photoionization and Charge Transfer Quenching

When the emitting level of the luminescent centers is degenerated in the conduction band, autoionization or photoionization usually occurs, resulting to a delocalization of the electron.

It may be free in the conduction band and recombine radiatively or nonradiatively through different processes and/or can be trapped in lattice defects. This process decreases the quantum efficiency of the luminescent ions and modifies the fluorescence kinetics giving rise, for example, to afterglow.

But the electron after ionization can be still bounded to the luminescent center, forming an exciton where the hole is located at the center. This exciton, known as impurity-bound exciton, can recombine radiatively and give rise to another kind of luminescence. This process can completely quench the luminescence of interest.

Some luminescent ions, namely rare-earth ions, when embedded in some crystals, may exhibit charge transfer transitions in the same energy range as transitions between localized states. After capture of an electron of the valence band, a charge transfer state can be formed which can partly or totally quench the luminescence, depending on its energy related to the one of the emitting level (see the case of Eu^{3+}-doped oxysulfides in Subchap. 3.6).

3.3.3.3 Concentration Quenching

Interaction between luminescent centers increases with their concentration in materials. Energy migration through nonradiative energy transfer can take place if the concentration is high enough. The excitation energy can travel over a long distance in the solid and reach a quenching site where it is lost nonradiatively. This phenomenon is called concentration quenching, and becomes effective for concentrations of few atomic percent of dopant ions. A very good example is given by CeF_3, which has a modest light yield in spite of a very high concentration of Ce^{3+} ions.

However, fully concentrated crystals can exhibit efficient luminescence. It is the case of very pure samples, which contain a very low concentration of killer centers. It is also the case of systems in which the luminescent ions show an emission with a large Stokes shift. As a result, the relaxed excited state is out of resonance with the neighboring ions and the energy migration cannot occur. Concentrated systems, which exhibit efficient scintillation, are, for example, $Bi_4Ge_3O_{12}$ (BGO) and CeF_3.

3.3.3.4 Reabsorption

The light emitted by luminescent centers comes out from the solid after a more or less long path over many lattice constants. It depends on the size and on the shape of the solid-state scintillator and on the configuration in which it is placed in the device using integrated techniques.

The luminescence traveling through the scintillator can be reabsorbed either by an identical or by different luminescent centers.

In the first case, the reabsorption is also called radiative energy transfer. This phenomenon leads to a lengthening of the fluorescence decay, but, in principle, does not affect the emission efficiency.

In the second case, the luminescence can be strongly quenched and the light yield of the scintillator substantially reduced. In large-size scintillators, reabsorption can be really an important limiting factor, and much care must be taken to grow transparent crystals in the wavelength region of luminescence. Many kinds of absorption centers can be present in crystals such as lattice distortions, point defects, color centers, etc. Using very pure starting materials, improvement of crystal growth, special annealing, etc., can reduce their number. It is often a big challenge to maintain a high light yield for large crystals of several tens of centimeters in length.

3.4 Creation and Quenching of Radiating Centers

In this paragraph, we will address a problem which has not received as much attention as the relaxation of the hot carriers and their thermalization but which has a strong impact on the parameters of scintillation; we discuss here the final stage of luminescent center excitation mechanism in scintillators under ionizing radiation. The final stages of the different scintillation mechanisms in inorganic compounds have been discussed briefly in Sect. 2.2. Here we focus our attention on oxide crystals doped with Ce^{3+} because the Ce^{3+} ion interconfiguration luminescence presumes the simultaneous presence of different excitation mechanisms [44]. The charge transfer excitation mechanism of the doping ion luminescence naturally appears from the fact that heterovalent Ce ions have a high cross section for capturing holes. Valbis [45] proposed this mechanism of scintillation for $YAlO_3$:Ce^{3+}. Another mechanism of scintillation, which we defined as energy transfer excitation mechanism, arises in oxide crystals where intrinsic luminescence centers exist. The bright scintillation through sensitizing of the Ce^{3+} luminescence occurs in complex structure oxide crystals, (1) which, when undoped, have an intrinsic excitonic luminescence from relaxed excited states; and (2) which, when Ce^{3+} doped, have a reasonable overlapping of the intrinsic matrix luminescence band and the activator absorption interconfiguration bands [46]. This mechanism had been recognized in Gd-based crystals [47, 48] and then in many other oxide compounds. A good evidence of the contribution of this mechanism in the scintillation of Ce^{3+}-doped Y and Lu-based crystals came up from experimental data. Table 3.1 shows the maxima of the intrinsic luminescence in several complex structure oxide crystalline compounds. Some of them, especially Y and Lu-based crystals, the technology of which is being extensively developed, have two characteristic intrinsic luminescence bands. These bands with maxima near 40,000 and 32,000 cm^{-1} (5 eV and 4 eV) are the common features of Al, Si, B, Be complex structure crystalline compounds. The short wavelength self-trapped exciton (STE) intrinsic luminescence band appears

Table 3.1. Peak maximum of intrinsic luminescence bands in some complex structure oxide crystals

Crystal	High-Energy Band Maximum (cm^{-1})	Low-Energy Band Maximum (cm^{-1})	Reference
$Y_3Al_5O_{12}$	39,200	33,600	13, 14
$YAlO_3$	44,800	33,600	7
Y_2SiO_5		33,200	15
$Lu_2Al_5O_{12}$		33,300	16
Lu_2SiO_5	39,060	31,750	9
$LuAlO_3$		31,350	1
Sc_2SiO_5		31,250	17
$Y_3Ga_5O_{12}$		32,800	18
Na_2ZrSiO_5		34,480–31,250	19
K_2ZrSiO_5		33,300	19
$K_2ZrSi_2O_7$		33,300	19
$Cs_2ZrSi_2O_7$		33,300–31,250	19
$Al_2Be_3Si_6O_{18}$	33,600	28,000	20
Al_2BeO_4	34,000	28,400	20
Be_2SiO_4	33,600	27,600	20
LiB_3O_5		32,800	21
$Li_2B_4O_7$		31,000	22

because of an interband transition $a_{1g}(\sigma) \rightarrow t_{1u}(\pi)$ and the long wavelength one is caused by radiative recombination of self-trapped holes STH [49]. The STE and STH luminescence intensity variations with temperature are opposite [50], so the thermodissociation of STE is an additional source of STH. A detailed examination of complex oxide compounds structure as well as results of EPR measurements [51] show that hole and excitons self-trapping occurs in oxygen sites of regular and slightly distorted oxygen polyhedra. The stabilization of O^--type centers and excitons near a vacancy in the heaviest cation site in complex compounds is considered as an alternative interpretation. However, it is inconsistent with the crystal growth peculiarities in the Y_2O_3–Al_2O_3 system. A strong aluminum oxide leakage from the melt is observed for perovskite crystal growth inducing Al vacancies in the crystal. The situation is even more dramatic in the case of $LuAlO_3$ where even a very small deficiency of Lu in the melt favors the growth of the garnet phase instead of the perovskite.

The combined luminescence of STE and STH gives a high light yield potential at room temperature in many complex structure crystals especially in oxides. For instance, both undoped $YAlO_3$ and $LuAlO_3$ show a wide luminescence band with maxima near 320 nm at room temperature, which is a superposition of the STE and STH luminescence. The total light yield of the scintillation exceeds 11,000 ph/MeV, while when the crystals is doped with cerium with concentration $\sim 10^{17} cm^{-3}$ or more, the STE and STH luminescence is

completely quenched in perovskites. It is a relatively rare situation when both intrinsic bands are quenched. In Ce-doped $Lu_2Al_5O_{12}$ and $Y_2Al_5O_{12}$ garnets, the quenching of STE luminescence arises only when the STH recombination and the Ce^{3+} interconfiguration emission have been observed simultaneously under ionizing radiation. Figure 3.7 shows excitation spectra of the Ce^{3+} luminescence in lutetium perovskite indicating sensitization of the Ce^{3+} luminescence by STE and STH. Besides Ce^{3+}interconfiguration $f \rightarrow d$ transitions in the range 200–320 nm, two peaks near 154 and 162 nm have been observed in luminescence excitation spectra. These bands are assigned, respectively, to the direct excitation of STE and STH in the crystal.

Besides STE and STH luminescence quenching, the Ce^{3+} impurity ion changes the conditions of holes self-trapping in the crystal. It is observed through excitation spectra in Ce-doped lutetium perovskite that the 162- nm (STH) excitation band is detected at near liquid helium temperature in integral excitation spectra, measured as a weak shoulder of the 154- nm band in low-temperature instantaneous spectra and disappears at room temperature. It is obvious that hole self-trapping in Ce-doped crystals is strongly suppressed because of the capture of the holes by the trivalent cerium ions.

Moreover, lutetium perovskite shows 75–84 nm excitation bands, which are due to transition from filled $4f^{14}$ shell of Lu^{3+} ion to the conduction band [53]. They are observed in instantaneous and integral measurement regimes, indicating that Ce^{3+} ions capture not only trapped but also "hot" holes from conduction band. Thus, the capture of the holes by Ce^{3+} plays a more significant role in the scintillation creation in lutetium than in yttrium-based crystals. This difference is also seen from the scintillation kinetics.

The scintillation kinetics is a single exponential in YAP:Ce and the decay constant of scintillation kinetics τ_{sc} is about the double of the radiation time of the luminescence kinetics under intracenter excitation τ_r. This is due to the slow STE and STH diffusion in a majority of complex structure oxide crystals based on light elements similar to Y [44]. On the contrary, Lu perovskite has a nonexponential scintillation kinetics that is rather well approximated with three exponents as seen in Fig. 3.8. The longest component is due to specific trap center in Lu perovskite. The shortest one is close to τ_r. The difference between τ_r and τ_{sc} of the initial part of the scintillation kinetics is a reasonable parameter to suggest this excitation mechanism of the radiating centers. A progressive change of the dominating excitation mechanism is observed in the $YAlO_3$–$LuAlO_3$ solid solution system when the Lu fraction is increased in the crystal. Figure 3.9 shows this variation of the fast scintillation component as a function of the substitution of Y by Lu in the crystal.

When the energy transfer excitation mechanism dominates [44], the light yield dependence on activator concentration is maximum. The maximum is determined by the STE diffusion rate and shifted to the higher concentration region for a slower diffusion. Such dependence is well recognized for

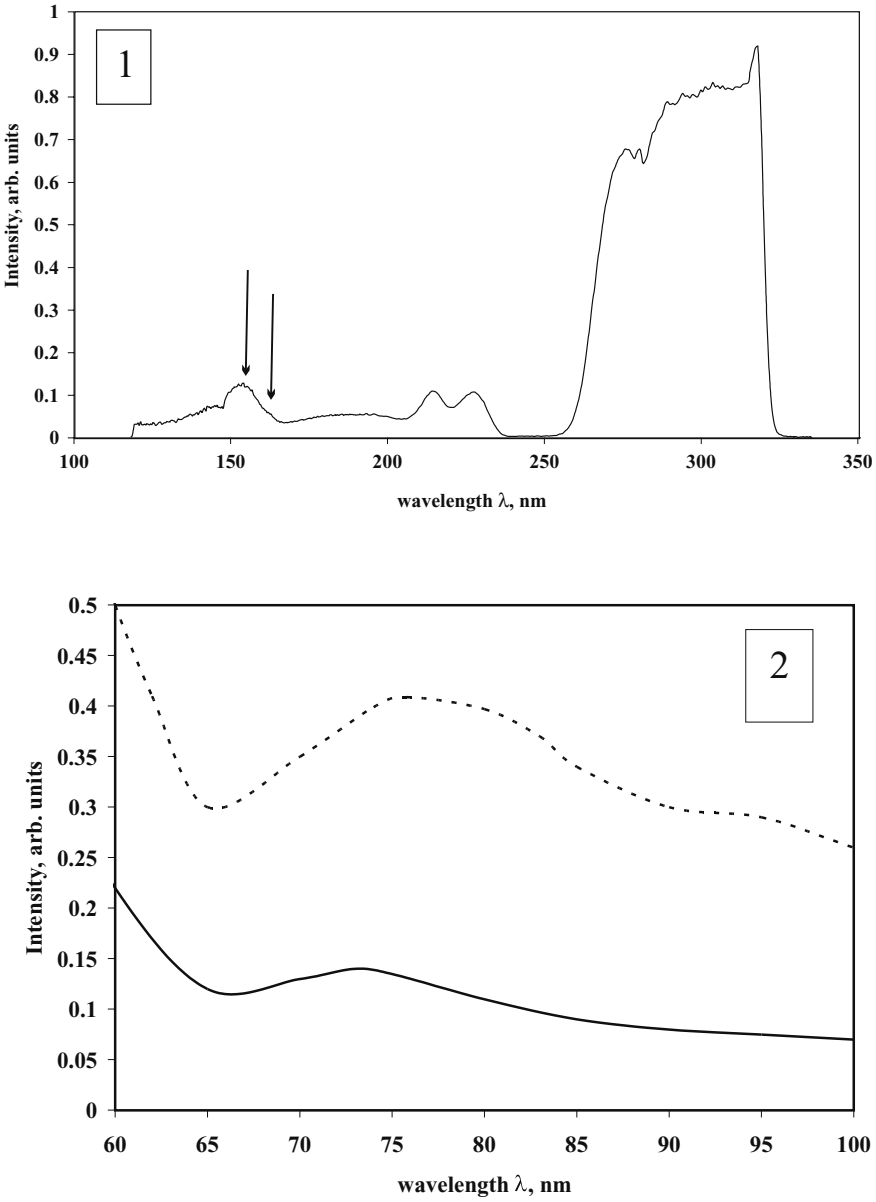

Fig. 3.7. Luminescence excitation spectra of Ce^{3+} luminescence ($\lambda_{lum} = 350$ nm) in $LuAlO_3$:Ce in the ranges 325–100 (1) and 100–60 (2) nm at 9°K. *Solid lines* represent spectra measured in integral regime and *dashed lines* are for spectra measured within 16 ns after excitation

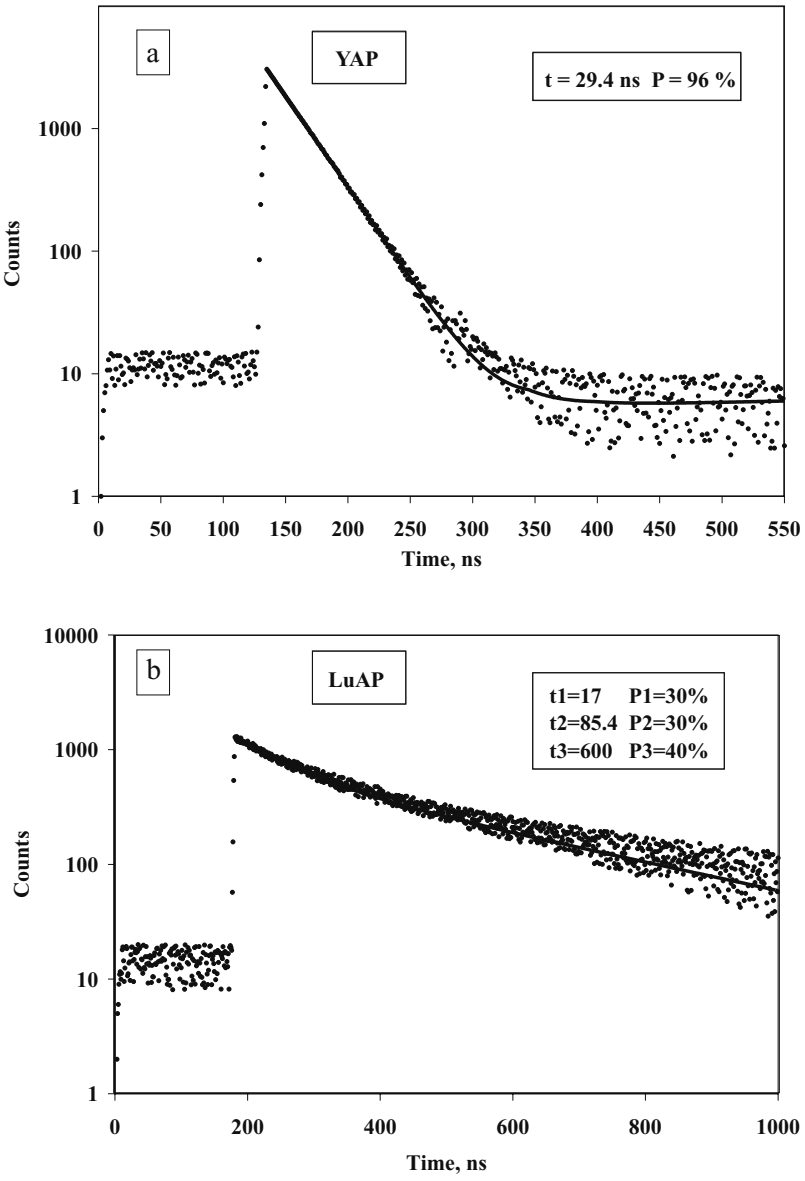

Fig. 3.8. Initial part of the scintillation kinetics of $YAlO_3$:Ce (**a**) and $LuAlO_3$:Ce (**b**) at room temperature (Pog scale)

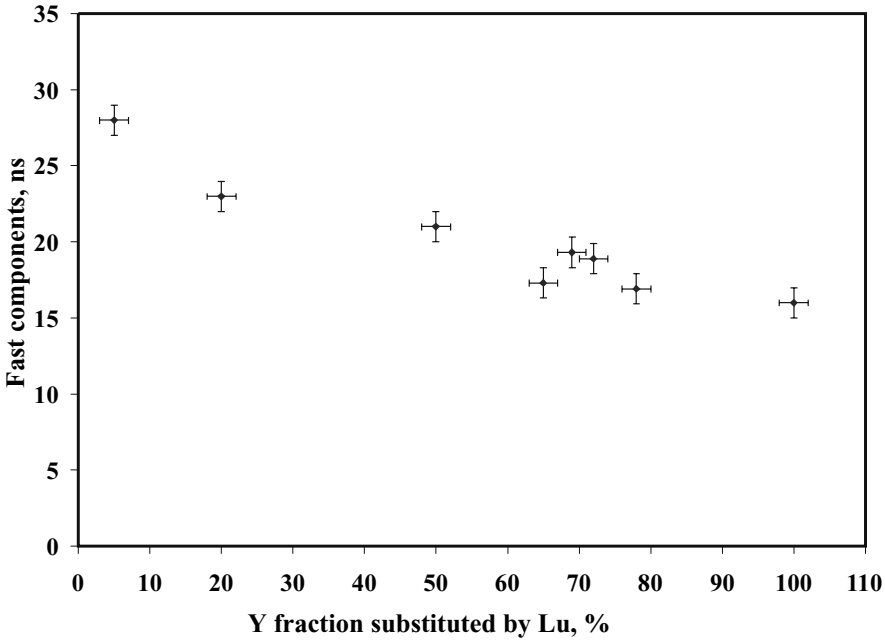

Fig. 3.9. Fast component of scintillation versus Y substitution by Lu in $(Y_{1-x}$–$Lu_x)AlO_3$:Ce, $T = 300\,K$

$YAlO_3$ and Gd_2SiO_5 doped with Ce^{3+}. Figure 3.10 shows the variation of the $YALO_3$:Ce light yield with the activator concentration.

In case of charge transfer excitation mechanism, the light yield dependence versus concentration has no maximum and reaches the saturation at relatively high activator concentration. It indicates that the scintillation light yield, where excitation charge transfer mechanism is prevailing, can be increased by an increase in the activator concentration. Figure 3.11 shows the variation of the $(Lu_{0.5}$–$Y_{0.5})AlO_3$:Ce light yield with the absorption coefficient of the maximum of the first allowed Ce^{3+} interconfiguration absorption band, which is proportional to the activator concentration. A similar dependence was seen in (Y–Lu)AlO_3 and $LuAlO_3$ crystals [54].

Both mechanisms of excitation show light yield temperature dependence strongly related to the presence of additional electron traps in the crystal. Figure 3.12 shows simulation results [44] of light yield temperature dependence for a perfect $YAlO_3$:Ce crystal (the temperature change of diffusion coefficient is taken into account) and for a crystal which has a shallow trap with a thermoactivation energy $E_{TA} = 0.2\,eV$ and a frequency factor $s \sim 1 \cdot 10^{12}\ s^{-1}$. In fact, shallow traps, at the relaxation stage, are additional sources of STE. Similar light yield temperature dependence is measured in different perovskite scintillation crystals [44, 55] (Fig. 3.13). A shift of the curve slope to the high-temperature region occurs because of an increase of

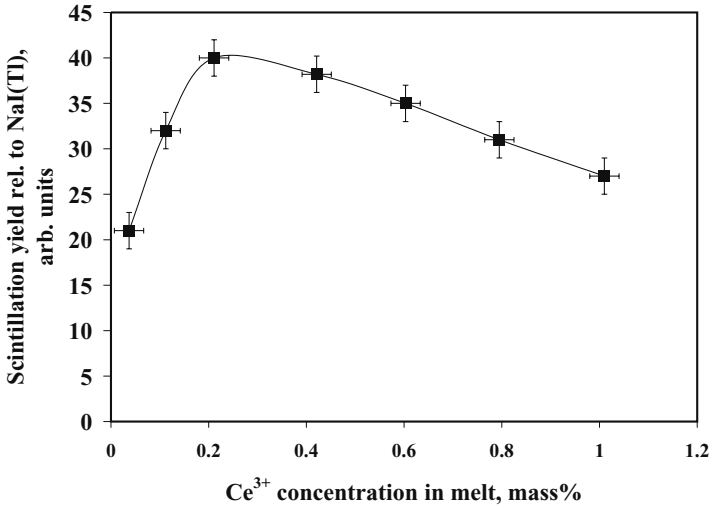

Fig. 3.10. Room temperature $YALO_3$:Ce light yield versus activator concentration

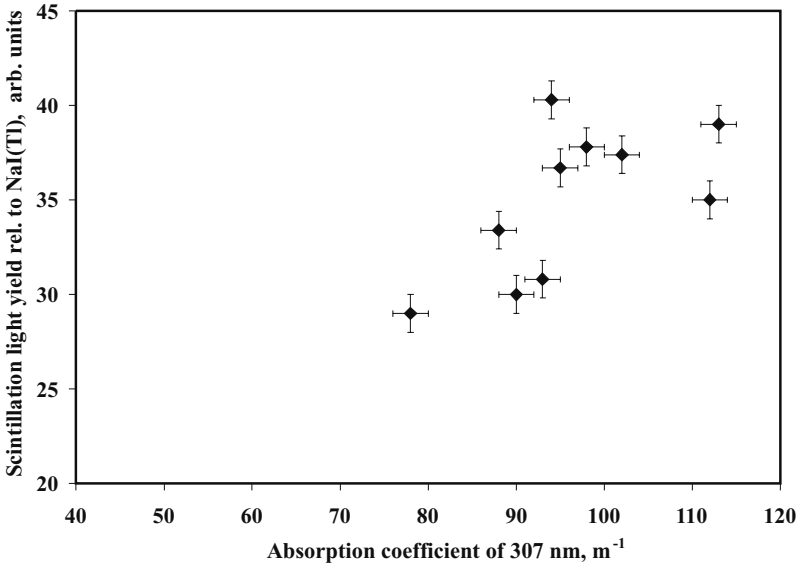

Fig. 3.11. Room temperature $(Lu_{0.5}–Y_{0.5})AlO_3$:Ce light yield versus absorption coefficient at 307 nm

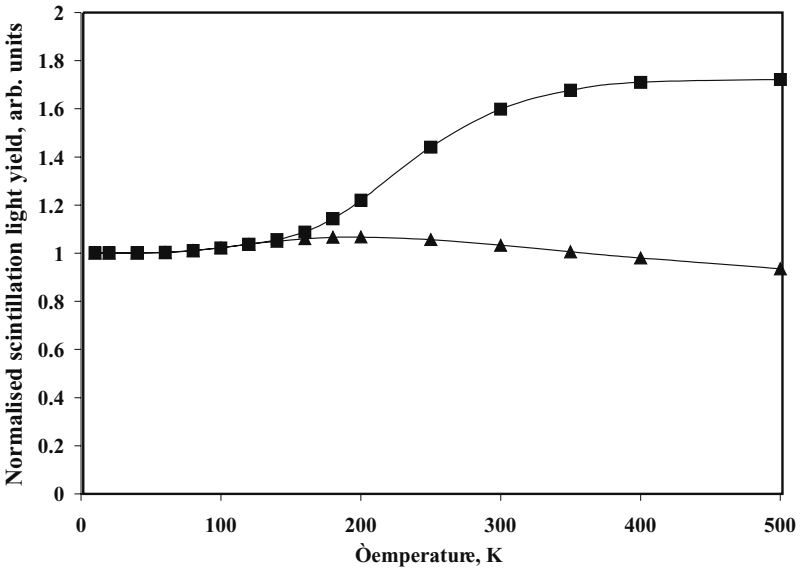

Fig. 3.12. Temperature dependence of the normalized scintillation light yield of $YAlO_3$:Ce in the case of no defect (triangle) in the crystal and crystal with one type of electron trap (square) for a middle slow diffusion of STE and activator concentration $\sim 10^{18}$ cm^{-3}

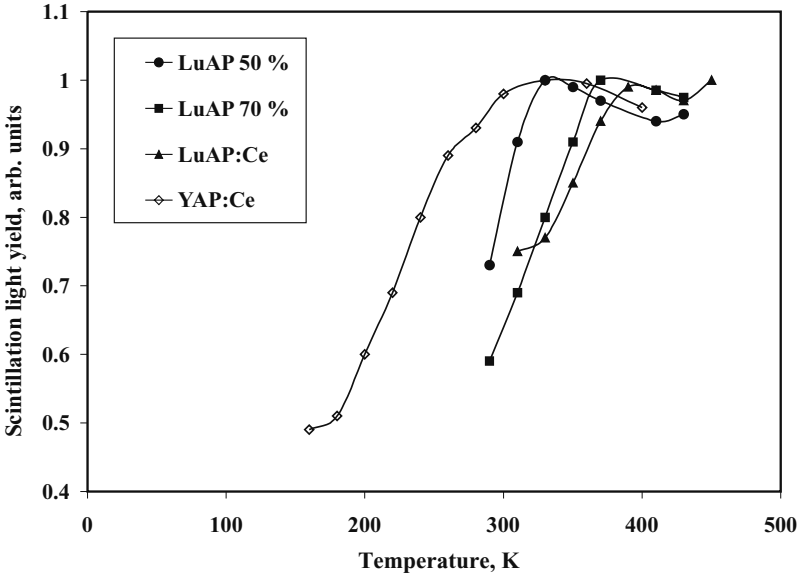

Fig. 3.13. Light yield temperature dependence in $YAlO_3$, $(Y_{0.5}–Lu_{0.5})AlO_3$, $(Y_{0.3}–Lu_{0.7})AlO_3$, $LuAlO_3$ crystals doped with Ce

the thermoactivation energy of the characteristic electronic center with an increase of the Lu fraction in the crystal. One can conclude that the variation of the electron trap centers concentration in YAP–LuAP crystals is an efficient way to control the crystal LY temperature dependence.

The determination of the radiating centers excitation mechanism is relatively obvious in crystals when the luminescence quantum yield is close to 1. However, in reality, synthetic crystals have specific defects and uncontrolled impurities, which very frequently introduce an additional quenching of the luminescence, and distort or even suppress the effective mechanisms of the radiating centers excitation. These quenching processes have to be minimized to achieve a high scintillation light yield. Not only the quenching of the intracenter Ce^{3+} luminescence has to be avoided but also the quenching of the STE by impurities and nonradiative STH relaxation has also to be suppressed.

3.5 Thermal Quenching

The luminescence thermal quenching phenomenon observed in luminescent centers embedded in a solid is always related to electron–phonon interaction and radiationless processes [3, 56].

To represent the electronic energy-level diagrams of the active ion by taking into account its interaction with the vibrating host lattice, the simplest model is the single-configurational coordinate (SCC) model.

This model considers only one vibration mode, a symmetrical stretching mode so-called breathing mode, described in the harmonic oscillator approximation. The configuration coordinate Q describes the vibration and represents the distance between the luminescent ion and the ligands. For more details, the reader can refer to the early work of Struck and Fonger [57] or to a review paper by Blasse [30].

This model is very convenient to describe thermostimulated processes leading to nonradiative recombination and thermal quenching of the luminescence.

3.5.1 Nonradiative Relaxation to the Ground State

A typical SCC diagram is represented in Fig. 3.14.

The energy E is plotted versus the coordinate Q. Potential curves of the ground state g and of one excited state e are represented by parabolas. The horizontal lines represent the vibration levels. The vertical lines indicate the optical transitions for which the probability is maximum (Franck Condon approximation). The equilibrium distance Q_g between the luminescent ion and the ligands, when the system is in its ground state, does not change during the absorption transition (Born-Oppenheimer approximation), but

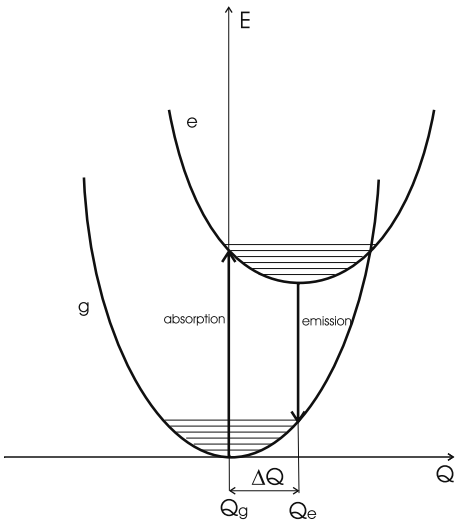

Fig. 3.14. The configurational coordinate diagram. The energy E is plotted versus the coordinate Q. The ground state g and one excited state e only are represented by potential curves with offset ΔQ. Absorption and emission transitions are indicated

changes into Q_e after relaxation of the excited state. The ion–ligand distance is, in general, larger in the excited state inducing parabolas offset. As a result, the emission transition from the relaxed excited state is shifted toward lower energy than the absorption transition (Stokes shift).

The Stokes shift is a measure of the interaction between the emitting center and the vibrating lattice. The larger is the Stokes shift the stronger is the electron–phonon coupling.

For weak coupling, the parabolas are not significantly shifted and the emission spectra show narrow lines (case of f–f transitions of rare-earth ions). In the case of intermediate coupling for which the parabolas are weakly shifted, vibronic spectra of broad emission lines are observed reflecting the progression in stretching vibration of the luminescent ion (case of uranyl pseudomolecules in oxides, such as UO_2^{2+}). Strong coupling leads to broad emission bands (case of mercury-like ions Tl^+, Pb^{2+}, Bi^{3+}, $5d \rightarrow 4f$ transitions of rare-earth ions, self-trapped excitons, molecular groups such as $(WO_4)^{2-}$, charge transfer transitions, etc.).

In the case of intermediate or strong coupling (Fig. 3.15a), the relaxed excited state may emit luminescence through radiative transition to the ground state. It may relax nonradiatively to the ground state if the temperature is high enough to allow the excitation to reach the crossing of the two parabolas.

This model accounts, therefore, for the thermal quenching of luminescence, and even for the total absence of luminescence at a given temperature when the Stokes shift is strong enough.

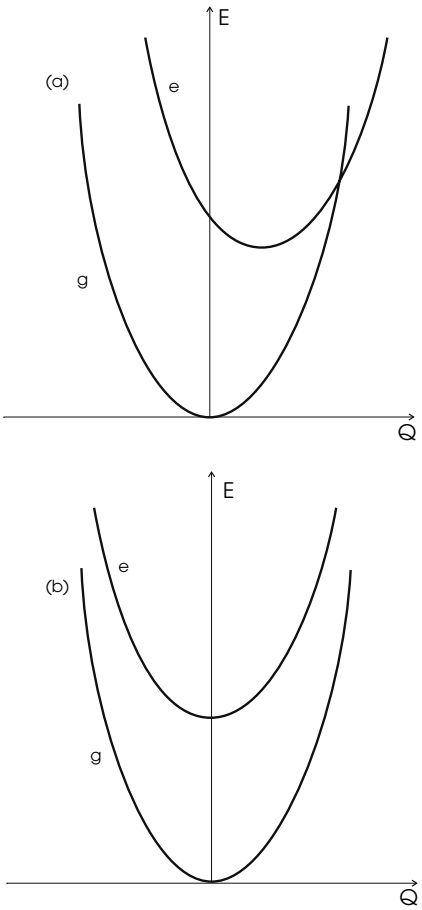

Fig. 3.15. Configurational coordinate diagrams illustrating (**a**) the case of intermediate/strong electron–phonon couplings and (**b**) the case of weak electron–phonon coupling

Many applications require use of scintillators at room temperature, and efficient scintillators must obviously contain luminescent centers with a quantum yield as close to 1 as possible without thermal quenching. It is, for example, the case of most Tl^+ or Ce^{3+}-doped scintillation crystals.

However, a particular case is the well-known BGO ($Bi_4Ge_3O_{12}$) scintillator for which the relatively low light output is essentially due to a room temperature quantum efficiency of only 0.13 because of thermal quenching [4].

There are cases where the thermal quenching may not have a harmful consequence. For example, $PbWO_4$ is a fast scintillator because of thermal quenching. Of course, its light yield is very weak as well, but it is nevertheless a good fast scintillator for some applications in high-energy physics for which

its interest is more related to the rapidity of the scintillation than to its efficiency.

Another interesting case is the Ce^{4+} center. Ce^{4+} is a full shell ion. No $4f$–$4f$ electronic transitions can occur because of empty $4f$ level. Nevertheless, charge transfer absorption transitions can be observed in the UV region but usually no radiative emission transitions due to a very large Franck Condon offset and a consequent crossover. Ce^{4+} is not a luminescent center. It often coexists with Ce^{3+} luminescent centers in cerium containing scintillating materials, and is a very harmful nonradiative recombination center.

Applications may require scintillators with high light output at temperature greater than room temperature. It is the case of oil well logging in which scintillation detectors are used to measure the natural or induced radioactivity of rocks. One of the most important requirements for borehole γ-ray detectors is the temperature response because of variable and relatively high borehole temperatures. Good candidates for such application are cerium-doped lutetium ortho-aluminates such as $LuAlO_3$ (LuAP) or $Lu_{1-X}Y_xAlO_3$ (LuYAP), and a new inorganic scintillator: cerium-doped lutetium pyro-silicate Ce^{3+}:$Lu_2Si_2O_7$ (LPS) [58] which all display a high light yield above room temperature.

In the case of very weak coupling ($4f$ levels of rare-earth ions), the parabolas are not significantly shifted (Fig. 3.15b). That does not mean that nonradiative relaxation to the ground state is impossible. It can occur through a so-called multiphonon nonradiative emission process. This process was first studied by Weber [59–61] and then by many other authors in a number of different rare-earth doped crystalline materials. It was demonstrated that spontaneous multiphonon emission rates strongly depend on the energy gap to the next-lower level (exponential energy gap dependence) and therefore on the number of phonons required to conserve energy (host dependence via phonon frequency spectrum). Nonradiative contribution to relaxation is significant even for large transitions corresponding to the simultaneous emission of 5–6 phonons.

In Fig. 3.16 is shown a schematic energy-level scheme of few rare-earth ions, where are indicated the emitting levels and which reflects the nonradiative relaxation rules previously described.

Blocks indicate higher energy configuration such as $4f^{n-1}$ $5d$ and charge transfer (CT). The energy of these levels strongly depends on the host lattice contrary to $4f$ levels. As a result, the emission from some $4f$ levels depends on the energy of lowest $5d$ or CT levels. For example, in the case of Pr^{3+}, the high-energy $4f$ ^1S_O level can emit fluorescence only when the $5d$ levels are located at higher energy. Reversely, $5d$ emission can be obtained only if the lowest $5d$ level is below ^1S_O. Indeed, Pr^{3+}-doped crystals may exhibit fast scintillation when Pr^{3+} ions are in the presence of a strong crystal field, which lowers the lowest $5d$ level. A large energy gap exists between the ground state and the $5d$ and CT lowest excited states of Ce^{3+} and Yb^{3+}, respectively. In

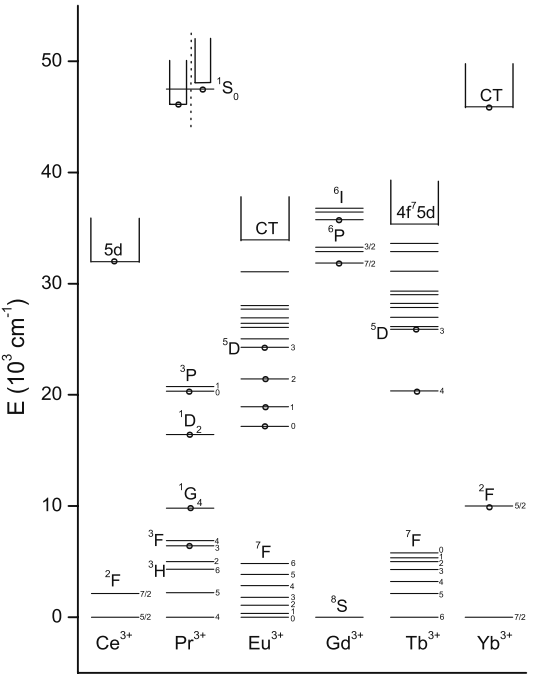

Fig. 3.16. Energy-level diagrams of some rare-earth trivalent ions. Circles indicate emitting levels. Blocks indicate levels of $4f^{n-1}5d$ and charge transfer (CT) higher energy configurations

principle, an efficient luminescence is expected if the Stokes shift is not too large.

3.5.2 Thermostimulated Photoionization and Trapping Effects

Photoionization of dopant ions in crystals can occur at relatively low energy when their localized ground and excited states are close or degenerated to/in the conduction band. This phenomenon may be of importance in luminescent and scintillating insulators because it may be the source of significant change in light efficiency and excited states dynamics. However, their importance was often underestimated in the past. It will be described in the next subchapter.

We will give here a few examples of thermostimulated photoionization.

Ce-doped Lu_2SiO_5 (LSO) is a well-known efficient scintillator at room temperature. Photoconductivity spectra obtained through direct photoconductivity measurements [62] and using the resonant microwave cavity technique [63–65] allow to estimate the energy difference between the bottom of the conduction band and the localized Ce^{3+} $5d$ emitting level. It is around a few tenths of eV, which still enable to observe significant photoconductivity

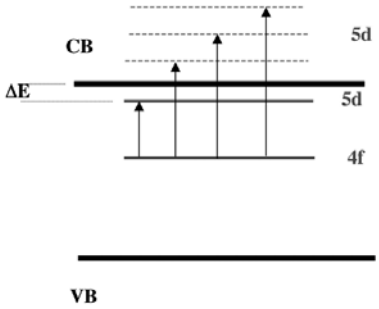

Fig. 3.17. Energy-level scheme of Ce^{3+} $4f$ and $5d$ levels in an ionic crystal. VB: valence band; CB: conduction band. The lowest $5d$ emitting level is lying in the forbidden gap close to the bottom of the conduction band, allowing thermostimulated photoionization

signal at room temperature through thermal activation. Figure 3.17 shows a simple energy-level scheme describing the process.

Similar results were obtained in the case of $Y_3Al_5O_{12}$:Ce. For using such scintillators at room temperature, it is therefore important to carefully control the temperature, because the light yield and the fluorescence decays are strongly temperature dependent. The efficiency drops down quickly and afterglow appears for temperatures slightly above room temperature.

The thermal quenching of scintillation of LaI_3:Ce crystal is explained by thermostimulated photoionization as well [66]. In this case, the lowest $5d$ state of Ce^{3+} is still closer (0.1 eV) to the bottom of the conduction band. As a result, this compound is a poor scintillator at room temperature but presents good scintillation properties for temperatures below 100°K.

Strong thermal quenching of scintillation may be the result of efficient trapping. This kind of quenching is observed only under excitation of the host lattice by ionizing radiations, and not under direct excitation of luminescent centers. It is due to the fact that high-energy excitation produces charge carriers, which may be trapped and cannot therefore excite luminescent centers, or only after a delay depending on the escape probability of trapped electrons which itself depends on temperature. In the temperature range where glow peaks are detected, revealing the presence of traps, a quenching of the scintillation is therefore expected and, as a consequence, a modification of the scintillation decay profiles.

Such trapping effects have been clearly identified in a number of scintillators. For example, ytterbium-containing YAG crystals exhibit X-ray–excited charge transfer luminescence. Its intensity drops drastically and its decay shows a very strong slow component at temperature below 120 K where thermoluminescence peaks are detected (Fig. 3.18) [37, 38]. The strong thermal quenching of X-ray induced emission of $LuBr_3$:Ce and $LuCl_3$:Ce observed

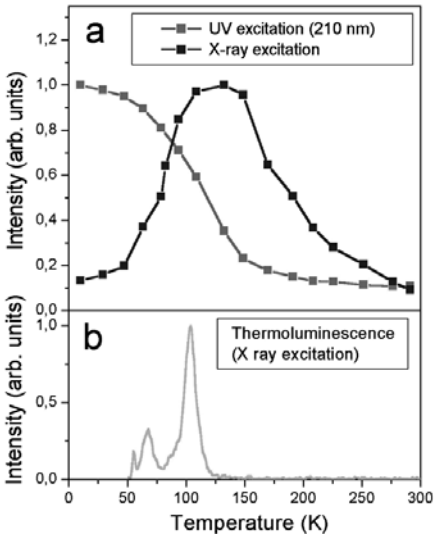

Fig. 3.18. Temperature dependence of the 333- nm integrated charge transfer emission band intensity (**a**), and thermoluminescence of YAG:Yb(50%) (**b**)

below 250 K is not understood by authors of [36] in the frame of their energy transfer model. It could be, however, interpreted by trapping effects as well.

3.6 Charge Exchange Processes Photoionization and Charge Transfer

To fully understand the electronic properties of a luminescent ion-crystal system, it is of importance to pay attention not only to localized transitions of the dopant ion, but also to charge exchange processes between the ion and the host crystal. In semiconductors, these exchange processes are the major phenomena while they are, in principle, of less importance in wide band-gap ionic crystals. However, their importance was underestimated too long, and it was demonstrated that they often occur in many transition metal and rare-earth ions activated compositions. When it is the case, these phenomena may lead to luminescence quenching of the dopant ion and may give rise to charge transfer luminescence. It is, therefore, of most interest to analyze them in doped scintillator crystals.

Photoionization and charge transfer of impurity ions in crystals are both dealing with electron transfer. They are, respectively, electron donor and electron acceptor transitions of the impurity. These processes were described using very simple phenomenological models. Jorgensen's formulation [67–69] later improved by Nakazava [70] was able to elucidate the systematic variation of the energies of CT transitions through the $4f^n$–series of rare-earth

ions. McClure and C. Pedrini used a simple electrostatic model to interpret the variation of the photoionization threshold of rare-earth impurity ions in crystals [71–73]. More recently, Thiel et al. [74] used photoemission spectroscopy for locating the energy of localized rare-earth impurity levels relative to host band structure in optical materials, and proposed an empirical model to describe the systematic trends of $4f$ binding energies.

3.6.1 Charge Transfer

Charge transfer can play a role in the luminescence process when the charge transfer states (CTS) are lying at relatively low energies close to the emitting levels of dopant ions (UV–visible region).

Energies of lowest charge transfer absorption transitions can be estimated by the empirical Jorgensen model:

$$\sigma = [\chi(X) - \chi(M)] \times 30,000 \text{ cm}^{-1} , \tag{3.3}$$

where $\chi(X)$ is the optical electron-negativity of the ligand anion and $\chi(M)$ is the optical electron-negativity of the central dopant ion. For ligands, $\chi(F) = 3.9$ [69], $\chi(O) = 3.2$ [75], $\chi(S) = 2.8$ [69].

Absorption bands are therefore expected at much higher energy in fluorides than in oxides, oxysulfides, and sulfides where CT transitions are usually observed in the UV–visible region.

Considering the case of rare-earth dopant ions in oxides, for example, in YPO_4 [70], Fig. 3.19 shows that Eu^{3+} (χ(Eu) = 1.75 [67]) and Yb^{3+} (χ = 1.6 [67]) are the ions for which the luminescence has the biggest chance to be perturbed by charge transfer states.

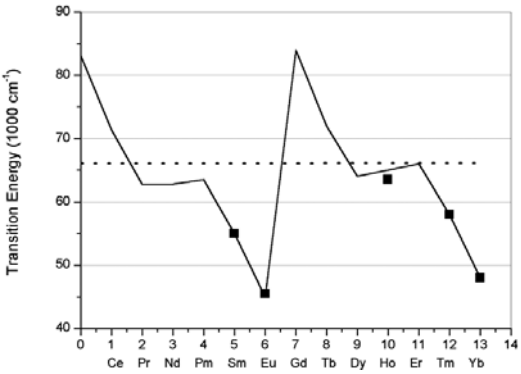

Fig. 3.19. Energy of the lowest charge transfer absorptions of rare-earth doped YPO_4 crystals. *Black squares*: experimental data; *solid line*: calculation; *broken line*: host lattice absorption edge

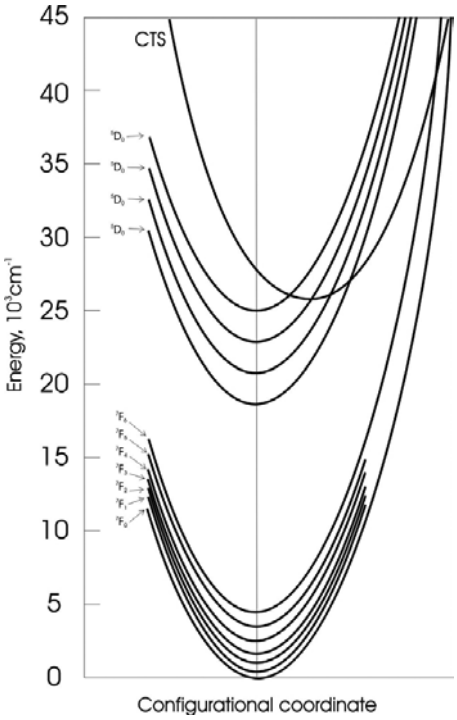

Fig. 3.20. Configuration coordinate diagram for the $4f$ and the lowest charge transfer state (CTS)of Eu^{3+}-doped Y_2O_2S, illustrating sequential quenching of ^5D emmissions

In Eu^{3+}-doped oxysulfides (La_2O_2S,Y_2O_2S), the minimum of the CTS is at rather low energy, leading to a strong sequential temperature-dependent quenching of ^5D_J emissions, as shown in Fig. 3.20 [76, 77].

This quenching depends, of course, on the host material. For example, the ^5D emissions quench sequentially in the order $^5D_3$, $^5D_2$, $^5D_1$, $^5D_0$ with increasing temperature, and corresponding quenching occurs at lower temperatures in the La compound. For Y_2O_3:Eu^{3+}, for which CTS bands are lying at much higher energies (about 10,000 cm^{-1} higher than in the oxysulfides), no thermally promoted $^5D \rightarrow$CTS transitions occur and no sequential quenching of the ^5D emissions are observed at temperature below 700°K.

In this case, it is possible to make use of CTS to efficiently absorb UV radiation and obtain strong red $^5D \rightarrow ^7F$ luminescence after nonradiative decay to the lower $4f$ levels. This red phosphor is used in fluorescent tubes.

It should be noted that in Eu^{3+}-doped materials, CTS emission is not observed because of radiationless relaxation through lower $4f$ excited states.

CT luminescence of Yb^{3+} is often observed in oxides and oxysulfides [78–80]. The electronic structure of Yb^{3+} is very favorable since the only

$4f^2F_{5/2}$ excited state is located around 10,000 cm^{-1} (1.25 eV) above the ground state $^2F_{7/2}$. Because of the large gap between the CTS and $^2F_{5/2}$ state, CT luminescence can be observed.

Recently, the observation of UV scintillation in yttrium/ytterbium aluminum garnets [81] opened the field of investigation to a new class of scintillating crystals with interesting fast luminescence properties, very attractive for radiation detection in general, and for neutrino physics, in particular [82], because of the high neutrino capture cross section by ytterbium. For this purpose, a detailed study of luminescence properties of ytterbium containing garnets and perovskites has been undertaken [36–38, 83, 84].

Localized levels of Yb^{3+} in the gap of the host and lowest CTS are presented in a single configuration coordinate diagram (Fig. 3.21).

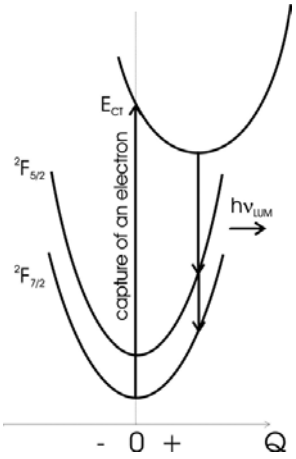

Fig. 3.21. Absorption and emission charge transfer transitions of Yb^{3+}-doped crystals using a simple configuration coordinate diagram

After capture of an electron from the ligands, a CTS is formed which can be described as an Yb^{2+} ion with a hole nearby in the valence band. Its potential curve has his minimum shifted toward larger Q corresponding to a larger Yb^{2+}-ligand ion equilibrium distance (Yb^{2+} radius > Yb^{3+} radius). If the shift is not too large, radiative relaxation is possible and then two broad emission bands separated by roughly 10,000 cm^{-1} (the energy difference between $^2F_{5/2}$ and $^2F_{7/2}$ states = 1.25 eV) are expected to be observed. For example, in the case of Yb^{3+}:YAG, the emission bands are peaking around 330 (the most intense) and 500 nm, and CT absorption occurs in the range 200–240 nm as predicted by the Jorgensen's model [37, 38].

CT luminescence of Yb^{3+}, because of its short radiative lifetimes (a few to a few tens of nanoseconds depending on the host lattice and the temperature) due to allowed transitions, is attractive for development of fast

scintillators capable to discriminate very short events. The fluorescence intensity can be high, but often thermal quenching processes occur below room temperature either due to cross-over from the CT-excited state to the ground state, or due to thermally activated photoionization involving the escape of a hole from the CTS to the valence band [81].

3.6.2 Photoionization

Photoionization of rare-earth ions in crystals has been observed and studied for $4f^n \rightarrow 4f^{n-1}\ 5d$ transitions. Indeed, the $4f^{n-1}\ 5d$ states can be close to the bottom of the conduction band and even degenerated within the continuum. In this case, the $5d$ electron can be delocalized in the conduction band resulting in a partly or complete quenching of the $4f^{n-1}\ 5d \rightarrow 4f$ luminescence.

It is why the first evidence of photoionization of rare-earth ions has been observed with divalent rare-earth ions and trivalent cerium ion, which usually exhibit $5d \rightarrow 4f$ luminescence [72–75, 85, 86]. Photoionization studies of impurity-doped crystals were motivated by the fact that their photo-physical properties were strongly dependent on photoionization process. It is the case for some potential solid-state laser materials such as CaF_2:Eu^{2+}, YAG:Ce^{3+}, crystals exhibiting persistent spectral hole burning like CaF_2:Sm^{2+}, and scintillator crystals of special interest here.

Photoionization processes particularly concern cerium-doped crystals, which are an important class of fast and efficient scintillators.

Let us consider the single configuration coordinate diagrams representing the localized levels of Ce in the gap of the host (Fig. 3.22).

Photoionization and CT energy thresholds can be calculated from thermodynamic cycles. In the case of Ce^{4+}, as previously mentioned, CT absorption and radiationless emission occur. In Ce^{3+}, $4f \leftrightarrow 5d$ transitions are usually observed in UV and visible range. Strong and fast luminescence may occur from the lowest $5d$-excited state providing this state is lying below the bottom of the conduction band, which is the case of the state ($Ce^{4+} + e_c$) in the diagram. This state is obtained after photoionization, e_c stands for an electron in the conduction band. Contrary to $Ce^{3+}5d$ excited states, the potential curve of ($Ce^{4+} + e_c$) is shifted toward negative Q since the Ce^{4+} ion radius is smaller than Ce^{3+} radius. The potential curve configuration represented in Fig. 3.22 corresponds to the case where the emitting level is lying well below the conduction band, and photoionization does not play any role in the luminescence process at room temperature (case of efficient cerium-doped scintillator crystals such as many Ce^{3+}-doped halides and oxides).

The opposite situation is when the lowest $5d$-excited state is degenerated in the conduction band. Then, the luminescence may be fully quenched even at low temperature due to autoionization. This is the case of cerium-doped sesquioxides (Ln_2O_3,Ln = La,Y,Lu) or some oxysulfides (La_2O_2S) [63].

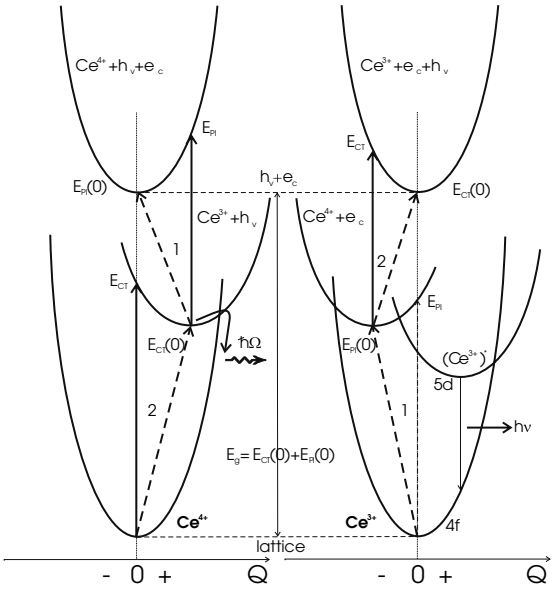

Fig. 3.22. Photoionization (1) and charge transfer (2) mechanisms of Ce^{3+} and Ce^{4+} ions embedded in crystal lattice, illustrated through single configuration coordinate diagrams

The intermediate case is when the emitting level is located closely below the bottom of the conduction band. Then, thermally assisted photo–ionization may occur leading to luminescence quenching at temperature below or above room temperature. The most efficient cerium-doped oxide scintillator at room temperature is Lu_2SiO_5:Ce (LSO), but its light yield rapidly decreases above room temperature. It was shown that the localized $5d$ level is located around only some tenths of eV below the conduction band, allowing photoionization even at room temperature through thermal activation [63]. $LaCl_3$:Ce^{3+} [36, 87–89] and $LaBr_3$:Ce^{3+} [90, 91] are scintillators with very high light yield, but LaI_3:Ce^{3+} exhibits efficient scintillation only at room temperature. The proximity of the Ce^{3+} lowest $5d$-excited state to the host conduction band leads to efficient autoionization process of Ce^{3+} above 150°K and therefore prevents any scintillation at room temperature [67].

The three cases are summarized in Fig. 3.23.

3.6.3 Impurity-Trapped Exciton

Electron-transfer transitions, in which an electron on the metal-impurity ion moves to lattice states, are not often observed. However, such transitions have been identified [73, 92, 93]. For example, in divalent rare-earth (Yb^{2+}, Eu^{2+}), doped, highly ionic crystals (such as alkaline earth fluorides), the so-called "anomalous" emission bands [94–99] were assigned to radiation from an

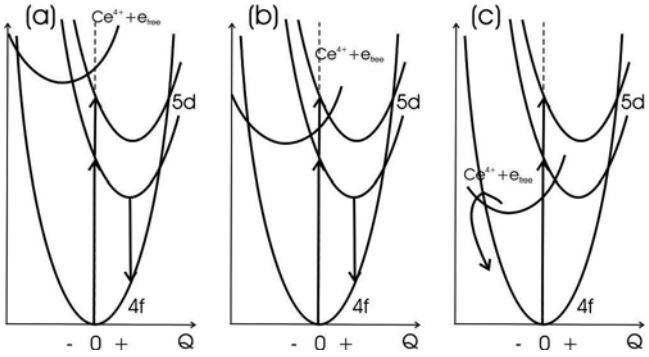

Fig. 3.23. Three scenarios for the fluorescence mechanisms of Ce^{3+} ions in crystals taking into account the state of the *bottom* of the conduction band (Ce^{4+} + e_{free}). (**a**) Intense fluorescence of Ce^{3+}. (**b**) Partly quenched fluorescence of cerium. (**c**) Total quenching of the Ce^{3+} fluorescence

impurity-centered exciton, which is the lowest excited state of the impurity-crystal system. Excitation of any of the localized levels of the impurity ion leads either to photoionization or to radiationless relaxation into lower levels. Normally, the lowest excited state localized level would be the emitting level, but when this level lies above the exciton energy it may relax into it, and the delocalized exciton may then emit instead.

For example, in the case of SrF_2:Yb^{2+} compound, the trapped exciton geometry is probably that expected for a trivalent impurity ion, Yb^{3+}, at a divalent site with an electron delocalized over the 12 next-neighbor metal–ion sites about 0.41 nm away. The collapse of the F^- cube around the Yb^{3+} could displace the F^- ions by about 0.02 nm, and would account for the large Stokes shift (Fig. 3.24).

It was demonstrated, through a detailed analysis of the fluorescence and the photoconductivity properties of Yb^{2+} in CaF_2, SrF_2 and BaF_2 [32], that all the 5*d* excited states of Yb^{2+} are degenerated in the conduction band, and that strong red shifted luminescence of ytterbium-trapped exciton is observed in CaF_2 and SrF_2. The negative shift of the exciton curve increases from CaF_2 to SrF_2 and even more for BaF_2. In the latter case, the shift is so large that the exciton relaxes nonradiatively to the ground state and no fluorescence at all is detected.

Impurity-trapped exciton luminescence has been observed in other systems such as titanium in sapphire [100] and BaF_2:Eu^{2+} [93].

This latter case is very interesting since Eu^{2+} ion in CaF_2 and SrF_2 exhibits typical and intense blue emission due to $5d \rightarrow 4f$ transitions while in BaF_2, a broad yellow emission band is detected because of europium-trapped exciton (Fig. 3.25).

The impurity-bound exciton model might be used to describe the fluorescence mechanisms in the well-known efficient CsI:Tl scintillator. A large

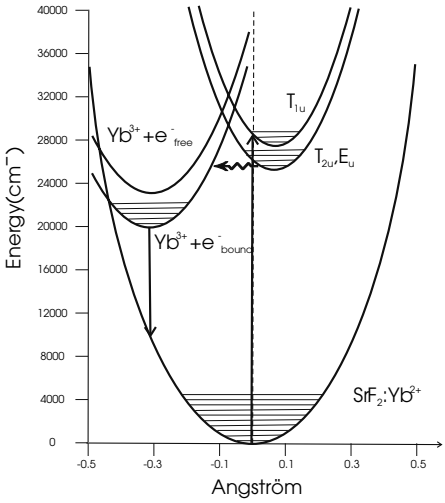

Fig. 3.24. Fluorescence mechanisms of ytterbium-bound exciton in Yb^{2+} doped SrF_2

number of publications deal with the origin of its yellow broad emission band and of its high light output. It comes out from the more recent studies that the centers emitting this fluorescence are of exciton type and related with thallium ions as well [101, 102]. These centers could be a host–exciton (the hole is in the valence band) with a thallium ion nearby, or a thallium-bound exciton (Tl^{2+} + e_{bound}) in which the hole is trapped in the thallium ion and the bound electron is delocalized in the neighboring Cs^+ ions, as it is sometimes the case in alkaline earth fluorides doped with divalent rare-earth ions.

It should be noted that the formation of impurity-bound exciton is strongly promoted when the impurity ion has two stable valence states such as Eu, Yb, Ti. It should be the case of Ce as well. However, no cerium-bound exciton fluorescence has been identified yet. It does not mean that such exciton state does not exist, because it can relax through a radiationless process to the ground state.

Because the exciton state lies below the bottom of the conduction band, its presence may induce a thermal quenching of the dopant ion fluorescence at lower temperature or a total quenching without photoionization depending on the relative positions of the localized states of the impurity ion, of the impurity-trapped exciton state, and of the bottom of the conduction band. But it may emit intense red shifted fluorescence with different properties, which can be of interest for scintillation.

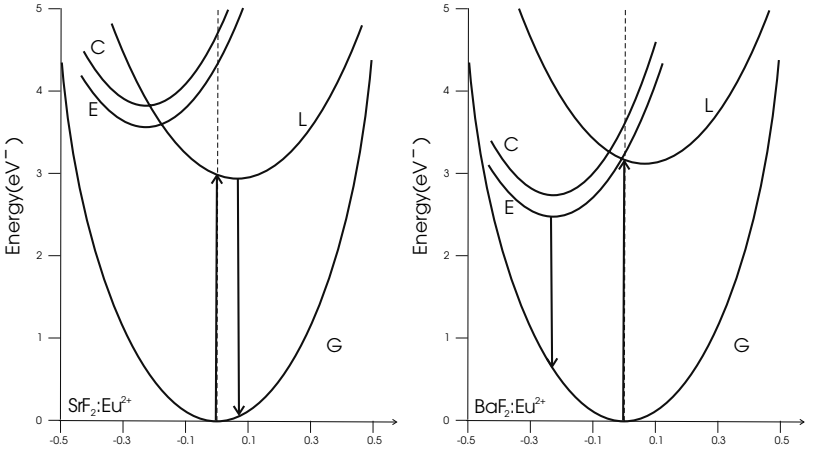

Fig. 3.25. Configuration coordinate diagram to explain the luminescence and photoconductivity spectra of SrF_2:Eu^{2+} and BaF_2:Eu^{2+}. The parabolas for the different states are the ground state G, a localized state L, the impurity-trapped exciton state E, the conduction band state C (Eu^{3+} + free electron). L is displaced outward by 0.1 Å. A and C are displaced inward by 0.2 Å. For G and L, $W = 0.04\,\text{eV}$ and for C and E, $W = 0.05\,\text{eV}$. The energy minima are placed according to spectroscopic data

References

1. Rodnyi PA, Dorenbos P, van Eijk CWE (1995) Energy loss in inorganic scintillators. Phys Stat Sol (b) 187:15–29
2. Bertram RH, Lempicki A (1996) Efficiency of electron–hole pair production in scintillators. J Luminescence 68:225–240
3. Vasil'ev AN (1996) Polarization approximation for electron cascade in insulators after high-energy excitation. Nucl Instr Meth Phys Res B 107:165–171
4. Lempicki A, Wojtowicz AJ, Berman E (1993) Fundamental limits of scintillator performance. Nucl Instr Meth Phys Res A333:304–311
5. Shockley W (1961) Problems related to p–n junctions in silicon. Solid State Electron 2:35–60
6. Klein CA (1968) Bandgap dependence and related features of radiation ionization energies in semiconductors. J Appl Phys 39:2029–2038
7. Pédrini C, Moine B, Gâcon JC, Jacquier B (1992) One- and two-photon spectroscopy of Ce^{3+} ions in LaF_3–CeF_3 mixed crystals. J Phys Condens Matter 4:5461–5470
8. Wojtowicz AJ, Berman E, Lempicki A (1992) Stoichiometric cerium compounds as scintillators, II. CeP_5O_{14}. IEEE Trans Nucl Sci 39:1542–1548
9. Nikl M, Mares JA, Mihokova E, Beitlerova A, et al. (1993) Energy transfer processes in CeF_3 single crystals. Solid State Com 87:185–188
10. Wojtowicz AJ, Balcerzyk M, Berman E, Lempicki A (1994) Optical spectroscopy and scintillation mechanisms of $Ce_xLa_{1-x}F_3$. Phys Rev B49:14880–14895

11. Williams RT, Thoma ED, Bunton PH (1994) Energy localization and decay in highly ionic crystals. Mater Res Soc Symp 348:331–342
12. Pédrini C, Belsky AN, Vasil'ev AN, et al. (1994) Fluorescence properties of CeF_3 and of some other cerium doped crystals and glasses under VUV and X-ray synchrotron excitation. Mater Res Soc Symp 348: 225–234
13. Wojtowicz AJ et al. (1994) Scintillation mechanism and radiation damage in $Ce_xLa_{1-x}F_3$ crystals. Mater Res Soc Symp 348: 455–461
14. Moses WN, Derenzo SE, Weber MJ, et al. (1994) Scintillation mechanisms in cerium fluoride. J Luminescence 59:89–100
15. Wojtowicz AJ et al. (1994) Scintillation light trapping and radiation damage in CeF_3. IEEE Trans Nucl Sci 41:713–718
16. Bouttet D, Dujardin C, Pédrini C, et al. (1996) X-ray photoelectron spectroscopy of some scintillating materials. In: Dorenbos P, van Eijk CWE (Eds) Proc Int Conf on Inorganic Scintillators and Their Applications, SCINT'95. Delft University Press, The Netherlands, pp 111–113
17. Pédrini C, Bouttet D, Dujardin C, et al. (1996) Energy transfer and quenching processes in cerium-doped scintillators. In: Dorenbos P, van Eijk CWE (Eds) Proc Int Conf on Inorganic Scintillators and Their Applications, SCINT'95. Delft University Press, The Netherlands, pp 103–110
18. Belsky AN, Glukhov RA, Martin P, et al. (1997) VUV excitation of intrinsic luminescence of ionic crystals with complicated band structure. Simulation. J Luminescence 72–74:96–97
19. Glukhov RA, Pedrini C, Vasil'ev AN (1997) Modelling of energy conversion and transfer in scintillators. In: Yin Zhiwen, Feng Xiqi, Li Peijun, Xue Zhilin (Eds) Proc Int Conf on Inorganic Scintillators and Their Applications, SCINT'97. CAS, Shanghai Branch Press, Shanghai, pp 111–114
20. Glukhov RA, Belsky AN, Pedrini C, Vasil'ev AN (1998) Simulation of energy conversion and transfer in CeF_3 after VUV photon absorption. J Alloys Compounds 275–277:488–492
21. Belsky AN, Kamenskikh IA, Mikhailin VV, et al. (1999) Energy transfer in inorganic scintillators. Rad Eff Defect S 150:1–10
22. Vasil'ev AN (2000) Relaxation of hot electronic excitations in scintillators: account for scattering, track effects, complicated electronic structure. In: Mikhailin VV (Ed) Proc of the Fifth Int Conf on Inorganic Scintillators and Their Applications, SCINT99. Moscow State University, Moscow, pp 43–52
23. Rodnyi PA (1992) Core-valence transitions in wide-gap ionic crystals. Soviet Phys Solid State 34:1053–1066
24. Belsky AN, Glukhov RA, Kamenskikh IA, et al. (1996) Luminescence quenching as a probe for the local density of electronic excitations in insulators. J Electron Spectrosc Relat Phenom 79:147–150
25. Terekhin MA, Vasil'ev AN, Kamada M, et al. (1995) Effect of quenching processes on the decay of fast luminescence from barium fluoride excited by VUV synchrotron radiation. Phys Rev B 52:3117–3121
26. Glukhov RA, Kamada M, Kubota S, et al. (1996) Effect of quenching processes on decay of fast luminescence from BaF_2. In: Dorenbos P, van Eijk CWE (Eds) Proc Int Conf on Inorganic Scintillators and Their Applications, SCINT'95. Delft University Press, The Netherlands, pp 204–205
27. Glukhov RA, Pedrini C, Vasil'ev AN, et al. (2000) Track effects in crossluminescence. In: Mikhailin VV (Ed) Proc of the Fifth Int Conf on Inorganic Scin-

tillators and Their Applications, SCINT99. Moscow State University, Moscow, pp 448–452
28. Chernov SA, Deych RG (1996) Luminescence mechanisms in CsI-based scintallators. In: Dorenbos P, van Eijk CWE (Eds) Proc Int Conf on Inorganic Scintillators and Their Applications, SCINT'95. Delft University Press, The Netherlands, pp 419–422
29. Chernov SA (1997) Relaxation of electron–hole pairs and scintillation mechanism in alkali halide crystals. J Luminescence 72–74:751–752
30. Blasse G (1988) Luminescence in inorganic solids: from isolated centers to concenterd systems. Prog Solid State Chem. 18:79–171
31. Wojtowicz AJ, Wisniewski J, Lempicki A, et al. (1995) Scintillation mechanisms in rare earth orthophosphates. Rad Eff Defect S. 135:305–310
32. Korzhik MV, Drobyskev GYu, Kondratiev DM, et al. (1996) Scintillation quenching in cerium-doped ytterbium-based crystals. Phys Stat Sol (b) 197:495
33. Blasse G, Schipper W, Hamelink JJ (1991) On the quenching of the luminescence of the trivalent cerium ion. Inorganica Chimica Acta 189:77–80
34. Pidol L, Kahn-Harari A, Viana B, et al. (2003) Scintillation properties of $Lu_2Si_2O_7$:Ce^{3+}, a fast and efficient scintillator crystal. J Phys Condens Matter 15:2091–2102
35. Pidol L, Guillot-Noël O, Jourdier M, et al. (2003) Scintillation quenching by Ir^{3+} impurity in cerium doped lutetium pyrosilicate crystals. J Phys Condens Matter 15:7815–7821
36. Guillot-Noël O, de Haas JTM, Dorenbos P, et al. (1999) Optical and scintillation properties of cerium-doped $LaCl_3$, $LuBr_3$ and $LuCl_3$. J Luminescence 85:21–35
37. Guerassimova N, Garnier N, Dujardin C, et al. (2001) X–ray–excited charge transfer luminescence in YAG:Yb and YbAG. J Luminescence 94–95:11–14
38. Guerassimova N, Garnier N, Dujardin C, et al. (2001) X-ray excited charge transfer luminescence of ytterbium-containing aluminium garnet. Chem Phys Lett 339:197–202
39. Glukhov RA, Vasil'ev AN (1995) Monte-Carlo simulation of the creation of excited region in insulators by a photon. Rad Eff Defect S 135:813–817
40. Glukhov RA, Vasil'ev AN (1994) Monte-Carlo study of energy losses in hot stage of electronic excitation relaxation in scintillators. Mater Res Soc Symp 348, pp 387–392
41. Pédrini C, Moine B, Bouttet D, et al. (1993) Time-resolved luminescence of CeF_3 crystals excited by X-ray synchrotron radiation. Chem Phys Lett 206:470–474
42. Belsky AN, Vasil'ev AN, Mikhailin VV, et al. (1994) Experimental study of the excitation threshold of fast intrinsic luminescence of CsI. Phys Rev B 49:13197–13200
43. Belsky AN, Cortes R, Gektin AV, et al. (1997) Excitation mechanisms of CsI fast intrinsic luminescence. J Luminescence 72–74: 93–95
44. Korzhik MV (2003) Physics of Scintillators on a Base of Oxide Compounds. Belarusian University, Minsk, p 263 (in Russian)
45. Averkiev VV, Valbis JA (1985) Luminescence Crystals and Convertors of Ionizing Radiation. Nauka, Novosibirsk, 1985, pp 30–35 (in Russian)
46. Korzhik MV, Trower WP (1995) Origin of scintillation in cerium doped oxide crystals. Appl Phys Lett 66: 2327–2328

47. Baryshevski VG, Kondratiev DM, Korzhik MV, et al. (1994) Mechanism of scintillation in Ce-doped gadolinium orthosilicate Gd_2SiO_5:Ce crystals. J Luminescence 60–61:956–959
48. Suzuki H, Tombrello TA, Melcher CL, et al. (1994) The role of the gadolinium in the scintillation processes of cerium- doped gadolinium oxyorthosilicate Nucl Instr Meth Phys Res A 346:510–521
49. Murk V, Kuznetsov A, Namozov B, Ismailov K (1994) Relaxation of electronic excitations in YAG and YAP crystals. Nucl Instr Meth Phys Res 91(1994):327–330 and references in the paper
50. Kuznetsov AI et al. (1982) Vacuum ultraviolet photo-luminescence of $YAlO_3$. Trudy Instituta Fiziki AN Estonskoi SSR 53:83–96 (in Russian)
51. Schirmer OF, Blazey KW, Berlinger W, Diehl R (1975) ESR and optical absorption of bound-small polarons in $YAlO_3$. Phys Rev B11:4201–4211
52. Cooke DW, Bennett BL, Muenchousen RE, et al. (2004) Intrinsic ultraviolet luminescence from Lu_2O_3, Lu_2SiO_5 and Lu_2SiO_5:Ce. J Luminescence 106:125–134
53. Dujardin C, Pedrini C, Gacon JC, et al. (1997) Luminescence properties and scintillation mechanisms of cerium- and praseodymium-doped lutetioum orthoaluminate. J Phys Condens Matter 9:5229–5243
54. Pedrini C, Dujardin C, Garnier N (2000) Proceedings of III Ural Workshop on Advantaged Scintillation and Storage Optical Materials, Ekaterinburg, Russia, pp. 3–29
55. Glodo J, Wojtowicz AJ (2000) Thermoluminescence and scintillation properties of LuAP and YAP. J Alloys Compounds 300–301: 289–294
56. DiBartolo B (1980) Radiationless Processes. Plenum Press, New York
57. Struck CW, Fonger WH (1975) Unified model of the temperature quenching of narrow-line and broad-band emissions. J Luminescence 10:1–10
58. Pidol L, Viana B, Kahn-Harari A, et al. (2005) Scintillation and thermoluminescence properties of $Lu_2Si_2O_7$: Ce^{3+} crystals. Nucl Instr Meth Phys Res A. 537:22–26
59. Weber MJ (1966) Relaxation processes for excited states of Eu^{3+} in LaF_3. In: Crosswhite HM, Moos HW (Eds) Optical Properties of Ions in Crystals. Interscience, New York, pp 467–484
60. Weber MJ (1967) Selective excitation and decay of Er^{3+} fluorescence in LaF_3. Phys Rev 156:231–241
61. Weber MJ (1967) Probabilities for radiative and nonradiative decay of Er^{3+} in LaF_3. Phys Rev 157:262–272
62. Yen WM, Raukas M, Basun SA, et al. (1996) Optical and photoconductive properties of cerium-doped crystalline solids. J Luminescence 69:287–294
63. Joubert MF, Kazanskii SA, Guyot Y, et al. (2003) A new microwave resonant technique for studying rare-earth photoionization thresholds in dielectric crystals under laser irradiation. Opt Mater 24:137–141
64. Guyot Y, Loudyi H, Kazanskii S, et al. (2004) rare-earth photoionization study by the resonant microwave cavity technique. Radiat Meas 38: 753–757
65. Joubert MF, Kazanskii SA, Guyot Y, et al. (2004) Microwave study of photoconductivity induced by laser pulses in rare-earth–doped dielectric crystals. Phys Rev B 69:165217
66. Bessière A, Dorenbos P, van Eijk CWE (2005). Luminescence and scintillation properties of the small band gap compound LaI_3:Ce^{3+}. Nucl Instr Meth Phys Res A 537:22–26

67. Jorgensen CK (1962) Electron transfer spectra of lanthanide complexes. Mol Phys 5:271–277
68. Jorgensen CK (1964) M.O. description of diatomic molecules containing a transition group atom. Mol Phys 7:417–424
69. Jorgensen CK (1971) Modern Aspects of Ligand Field Theory. North-Holland, Amsterdam
70. Nakazawa E (2002) The lowest $4f$-to-$5d$ and charge-transfer transitions of rare-earth ions in YPO_4 hosts. J Luminescence 100:89–96
71. Pédrini C, Mc Clure DS, Anderson CH (1979) Photoionization thresholds of divalent rare-earth ions in alkaline earth fluorides. J Chem Phys 70:4959–4962
72. Mc Clure DS, Pédrini C (1985) Excitons trapped at impurity centers in highly ionic crystals. Phys Rev B32: 8465–8468
73. Pédrini C, Rogemond F, Mc Clure DS (1986) Photoionization thresholds of rare-earth impurity ions. Eu^{2+}:CaF_2, Ce^{3+}:YAG, and Sm^{2+}:CaF_2. J Appl Phys 59:1196–1201
74. Thiel CW, Crugnel H, Wu H (2001) Systematics of $4f$ electron energies relative to host bands by resonant photoemission of rare-earth ions in aluminum garnets. Phys Rev B64:085107
75. Vugt N, Wigmans T, Blasse G, et al. (1973) Electron transfer spectra of some tetravalent lanthanide ions in ZrO_2. J Inorg Nucl Chem 35:2601–2602
76. Struck CW, Fonger WH (1970) Role of the charge-transfer states in feeding and thermally emptying the ^5D states of Eu^{+3} in yttrium and lanthanum oxysulfides. J Luminescence 1–2:456–469
77. Struck CW, Fonger WH (1971) Dissociation of Eu^{+3} charge-transfer state in Y_2O_2S and La_2O_2S into Eu^{+2} and a free hole. Phys Rev B4:22–34
78. Nakazawa E (1978) Charge-transfer type luminescence of Yb^{3+} ions in $LuPO_4$ and YPO_4. Chem Phys Lett 56:161–163
79. Nakazawa E (1979) Charge transfer type luminescence of Yb^{3+} ions in RPO_4 and R_2O_2S (R=Y, La, and Lu). J Luminescence 18–19: 272–276
80. Van Pieterson L, Heeroma M, de Heer E, et al. (2000) Charge transfer luminescence of Yb^{3+}. J Luminescence 91:177–193
81. Bressi G, Carugno G, Conti E (2001) New prospects in scintillating crystals. Nucl Instr Meth Phys Res A 461:361–364
82. Chipaux R, Cribier M, Dujardin C, et al. (2002) Ytterbium-based scintillators, a new class of inorganic scintillators for solar neutrino spectroscopy. Nucl Instr Meth Phys Res A 486:228–233
83. Kamenskikh IA, Guerassimova N, Dujardin C, et al. (2003) Charge transfer fluorescence and f-f luminescence in yttrium compounds. Opt Mater 24:267–274
84. LUMDETR 5th European Conference on Luminescent Detectors and Transformers of Ionizing Radiation, Sept. 1–5 (2003), Pargue, Czech Republik, abstract book p. 17
85. Pédrini C, Pagost PO, Madej C, et al. (1981) Photoconductivité due à l'autoionisation de Ce^{2+} dans CaF_2, SrF_2 et BaF_2. J de Phys 42: 323–330
86. Pédrini C, Gaume-Mahn F, Mc Clure DS (1982) Photoconductivity due to autoionization of divalent rare-earth impurities in crystals having the fluorite structure. In: Mc Carthy GJ, Siber HB, Rhyne JJ (Eds) The Rare Earths in Modern Science and Technology, vol 3, pp 165–169
87. Blasse G, Schipper W, Hamelink JJ (1991) On the quenching of the luminescence of the trivalent cerium ion. Inorg Chim Acta 189:77–80

88. Van Loef EVD, Dorenbos P, van Eijk CWE, et al. (2000) High-energy–resolution scintillator: Ce^{3+}activated $LaCl_3$. Appl Phys Lett 77:1467–1468
89. Van Loef EVD, Dorenbos P, van Eijk CWE, et al. (2001) Scintillation properties of $LaCl_3$:Ce^{3+} crystals: fast, efficient, and high-energy resolution scintillators. IEEE Trans Nucl Sci 48:341–345
90. Van Loef EVD, Dorenbos P, van Eijk CWE, et al. (2001) High-energy–resolution scintillator: Ce^{3+} activated $LaBr_3$. Appl Phys Lett 79:1573–1575
91. Van Loef EVD, Dorenbos P, van Eijk CWE, et al. (2002) Scintillation properties of $LaBr_3$:Ce^{3+} crystals: fast, efficient and high-energy–resolution scintillators. Nucl Instr Meth Phys Res A 486:254–258
92. Moine B, Courtois B, Pédrini C (1989) Luminescence and photoionization processes of Yb^{2+} in CaF_2, SrF_2 and BaF_2. J Phys France 50:2105–2119
93. Moine B, Pédrini C, Courtois B (1991) Photoionization and luminescences in BaF_2:Eu^{2+}. J Luminescence 50:31–38
94. Kaplyanskii AA, Smolyanskii PL (1973) Polarized luminescence of CaF_2–Yb^{2+} crystals. Opt Spectrosc 34 :361–362
95. Rent EG (1976) Luminescence of divalent Eu and Yb ions in fluorite-type crystals. Opt Spectrosc 40:55–57
96. Kaplyanskii AA, Medvedev VN, Smolyanskii PL (1976) Spectra, kinetics, and polarization of the luminescence of CaF_2–Yb^{2+} crystals. Opt Spectrosc 41:615–619
97. Zapasski VS, Feofilov PP (1976) Magneto-optical studies of the radiative state of divalent ytterbium in fluorite crystals. Opt Spectrosc 41:620-622
98. Kaplyanskii AA, Medvedev VN, Smolyanskii PL (1977) Stress polarization of luminescence and the structure of emitting states of CaF_2–Yb^{2+} crystals. Opt Spectrosc 42:74–78
99. Rent EG (1978) Characteristics of the broadband luminescence of Eu and Yb ions in crystals with the flurite structure. Opt Spectrosc 45:291–294
100. Wong WC, Mc Clure DS, Basun SA, et al. (1995) Charge-exchange processes in titanium-doped sapphire crystals. II. Charge-transfer transition states, carrier trapping, and detrapping. Phys Rev B51:5682–5698
101. Spaeth JM, Meise W, Song KS (1994) The nature of the X-ray–induced luminescence and the hole centers in CsI:Tl studied by optically detected electron paramagnetic resonance. J Phys Condens Matter 6:3999–4008
102. Nikl M (2000) Wide band gap scintillation materials: Progress in the technology and material understanding. Phys Stat Sol (a) 178:595–620